UNIVERSITY OF CALIFORNIA,
IRVINE

ICCD Camera Based Temperature Modulated Fluorescence Tomography

THESIS

submitted in partial satisfaction of the requirements
for the degree of

MASTER OF SCIENCE

in Biomedical Engineering

by

Deniz Nikkhah

Thesis Committee:

Associate Professor Gultekin Gulsen, Chair
Associate Professor Jered Haun
Assistant Researcher Farouk Nouizi

2022

DEDICATION

To

my family, mentors, and friends

in recognition of their support

for believing in me

and

supporting me through this path.

"There is a fundamental difference between religion, which is based on authority, and science, which is based on observation and reason. Science will win because it works."
— Stephen Hawking

TABLE OF CONTENTS

LIST OF FIGURES

ACKNOWLEDGEMENTS

I would like to express my gratitude to the TM-FT core team members and acknowledge their work. Mentoring efforts of my committee chair Dr. Gultekin Gulsen, and assistance of Dr. Farouk Nouizi, made this project feasible.

I would like to express my appreciation to my committee chair, Professor Gultekin Gulsen who continuously encourages me and has faith in me. Without his guidance and persistent help this thesis would not have been possible. There aren't many faculty advisors who are as concerned about their students as they are about their research projects, and I feel incredibly lucky to have Dr. Gultekin Gulsen unconditional support as my research advisor. He showed me how to solve challenges with consistency and creativity. Thank you, Dr. Gultekin Gulsen, for always being supportive when I had a problem. I greatly appreciate all your assistance, especially the time you spent in the lab instructing and guiding me.

I would also like to thank my committee members, Dr. Jered Haun, and Dr. Farouk Nouizi. You have been a source of inspiration and role model for many people. Thank you for all your assistance, suggestions, and training. Thank you for your insights and serving on my committee. Without your support and guidance this project and this thesis would not be feasible. Dr. Nouizi also helped me tremendously with experimental setup design and image reconstruction. Therefore, I would like to thank him again for all his hard work, support and insightful feedbacks.

I also want to thank the S-STEM program for their funding support through this path, without their support my degree completion would not be as easy; and lastly, I want to thank my parents, family and friends for their unconditional support and encouragement through my academic path and importantly having faith on my future.

ABSTRACT OF THE THESIS

ICCD Camera Based Temperature Modulated Fluorescence Tomography

by

Deniz Nikkhah

Master of Science in Biomedical Engineering

University of California, Irvine, 2022

Associate Professor Gulsen Gultekin, Chair

Fluorescence diffuse optical tomography (FDOT) is one of the most sensitive imaging modalities used in whole-body preclinical research. It offers 3D distribution of endogenous tissue contrast, fluorescent proteins, and exogenous fluorescent contrast agents. The main obstacle to its clinical application has been its low spatial resolution, despite its higher sensitivity. This limitation is mostly caused by the high optical photon scattering in biological tissue and the insufficient surface measurements, which result in an ill-posed and underdetermined inverse problem. An innovative technique known as Temperature Modulated Fluorescence Tomography (TMFT) is earlier introduced by our research group to address these shortcomings of FDOT. Thermo-sensitive fluorescent agents (ThermoDots) are one of the key components of TMF in addition to high-intensity focused ultrasound (HIFU), which is employed to locate these ThermoDots. The distribution of the ThermoDots can be determined with great spatial accuracy by scanning the tissue with a focused HIFU beam (Ø =1.3 mm), while measuring the fluctuation in the

detected fluorescence signals. A prototype TMFT system that makes use of optical fibers for detection has already been constructed previously by our group. Unfortunately, this fiber-based system necessitates submerging the animal in optical matching fluid. In this study, we propose an improved version that enables non-contact imaging using a ICCD camera-based detection and removes the requirement of submerging the animal by placing it on an ultrasonic transparent membrane. Performance validation studies using tissue simulating phantoms show that high spatial-resolution (~ 1.3 mm) and superior quantitative accuracy in recovered fluorophore concentration (<3% error) can be obtained using this new version. This ICCD-based TM-FT system will pave the way for the practical and widespread application of TM-FT in preclinical research.

CHAPTER 1: Diffuse Optical Tomography (DOT)

Variety of imaging modalities can provide structural, functional and/or molecular information in vivo using a broad spectrum of technologies. Structural imaging allows visualization of anatomic structures, while functional imaging provides physiological state of the tissue. Ultrasound, X-ray Computed Tomography and Magnetic Resonance Imaging (MRI) have been primarily used to provide images of the structure for long time. On the other hand, nuclear and optical imaging modalities can exclusively provide functional and molecular information. Their sensitivity is also higher and therefore, they have a great potential to detect the abnormalities based on the subtle changes in the tissue physiology prior to the anatomical changes detected by structural imaging modalities. Compared to nuclear imaging, in vivo optical imaging is relatively new and possesses the advantage of utilizing low-cost instrumentation and non-ionizing radiation that is safe for the biological tissues. Furthermore, production cost of optical contrast agents is much less, and their distribution is much more convenient due to their long shelve-life. In vivo optical imaging extends across a wide range of resolution, from molecular and cellular to tissue and organ levels. At the higher end of the spectrum, diffuse optical tomography (DOT) is an emerging non-invasive imaging technique that uses near-infrared light to recover the optical parameter maps of the thick tissue under investigation.

DOT offers the opportunity to image three-dimensional (3-D) spatial variations in blood parameters, particularly hemoglobin concentration and oxygen saturation, and thus metabolic factors which these concentrations reflect, along with tissue scattering

characteristics. The instrumentation is noninvasive, nonionizing, inexpensive. DOT can provide images up to several cm depth. An array of near-infrared (NIR) light sources provides illumination at the surface of tissue, and an array of photodetectors surrounds the volume under investigation to detect the transmitted and reflected light from tissue. NIR light is used to achieve DOT within the diagnostic–therapeutic window which enables the recovery of the internal distribution and concentration of tissue chromophores via tomography [1]. By measuring the fluence rate on the tissue surface, DOT attempts to recover the spatial distribution of optical/physiological properties in the tissue. The DOT algorithm mainly consists of two parts: the forward model, which simulates how light propagates in the tissue and estimates synthetic measurements at the tissue boundary. The inverse solver, on the other hand, attempts to recover the optical property distribution by minimizing the difference between the estimated synthetic and real measured data.

1.1 Modeling of the light interaction with tissue and image reconstruction in DOT

Absorption and scattering are two fundamental interactions that can occur as photons move through biological tissue [2]. The main optical properties of the medium that explain its interaction with light are described in this section: absorption, and scattering. For the development of optical tools for diagnosis and treatment, understanding light propagation is essential. Since the optical photons cannot propagate through biological tissue in a straight line due to light scattering, image reconstruction in diffuse optical tomography is

very challenging. The two models for light propagation that are most frequently employed are the radiative transfer equation (RTE) and diffusion equation (DE) for DOT[3].

Photons can be absorbed by the medium as they pass through tissue. Eq. 1 The Beer-Lambert law, which relates the amount of light attenuation to the properties of the material, can be used to explain this attenuation or reduction of light as it propagates through a non-scattering medium:

$$I = I_o e^{-\mu_a(\lambda)x} \quad (1)$$

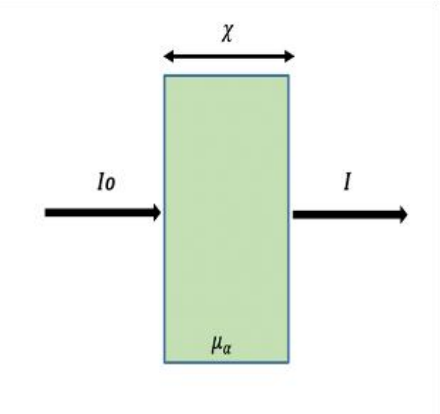

Figure 1.1: The Illustration of light attenuation through an absorbent medium.

As shown in Figure 1.1, I0 is the incident light intensity, I is the measured intensity after propagation through a tissue of thickness x, and $\mu a\ (\lambda)$ is the medium's absorption coefficient. The likelihood of a photon being absorbed per unit length in a particular material is represented by the absorption coefficient $\mu a\ (\lambda)$. *Its* reciprocal, the free path of absorption $1/\mu a\ (\lambda)$, can be thought of as the maximum distance a photon can travel before being absorbed in a material [4]. The absorption coefficient describes a type of absorber (chromophore) and is determined by the concentration of the chromophore, C[M], and the wavelength (λ) of light used as shown in Eq 2.:

$$\mu(\lambda) = \ln 10 \cdot \varepsilon(\lambda) \cdot C \quad (2)$$

where εn(λ) is the wavelength-dependent extinction coefficient, which describes a chromophore's absorption at a specific wavelength. A single chromophore or a combination of chromophores can cause the absorption coefficient to change. As illustrated by Eq.3 the sum of the absorption coefficients of each chromophore can be used to calculate the overall absorption coefficient:

$$(\lambda) = \ln 10 \cdot \sum_n \varepsilon_n (\lambda) \cdot C_n \quad (3)$$

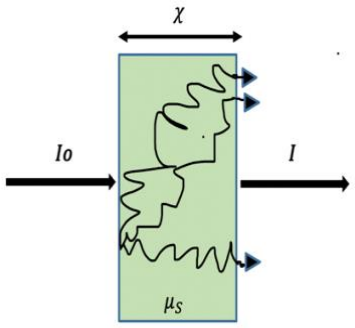

Figure 1.2: Illustration of light attenuation through a highly scattering medium.

In addition to absorption, a photon can scatter while traveling through biological tissue. Scattering occurs when the refractive index of small barriers, such as cell membranes, differs. The photon does not go out of the tissue borders, but it does change its orientation because of interaction with tissue constituents as illustrated in Figure 1.2. The likelihood of a photon being scattered per unit length is called the scattering coefficient μs*, which* describes the scattering of a medium. The free path of scattering, 1/μs, is the distance a photon can travel before being dispersed in a material. If the medium is heavily scattering, the photons' pathways are no longer straight lines resulting in a significant diffusion of light across the medium. The photons emerge from the medium at diverse places and directions due to the different photon. Furthermore, because each photon travels a distinctly different distance due to scattering, calculating the attenuation of light in a substance that is both absorbing and scattering, such as biological tissue, is particularly difficult.

It is commonly acknowledged that the RTE, which is based on the law of conservation of energy, accurately represents light propagation in biological tissue when it passes through a medium comprising absorbers and scatterers [3].The expression for the time-domain (TD) RTE is shown in Eq 4.:

$$\left[\frac{\delta}{v(\mathrm{r})\delta t} + \Omega.\nabla + \mu_a(\mathrm{r}) + \mu_s(r)\right] I(\mathrm{r},\Omega,t) = \mu_s(\mathrm{r}) \int_{4\pi} d\,\Omega' P(\mathrm{r},\Omega.\Omega') I(\mathrm{r},\Omega,t) + q(\mathrm{r},\Omega,t) \qquad (4)$$

In RTE function I (r, Ω, t) is light radiance. Moreover, light is lost through divergence and extinction due to photon absorption and scattering away from the propagation direction Ω'. μa and μs are absorption and scattering coefficients. Light gain from scattering through the medium and internal light source are described by q (r, Ω, t) and the phase shift is respectively described by the term P (r, Ω, t).

The RTE is an integro-differential equation, which makes it challenging to solve analytically and exceedingly computationally intensive for numerical solutions. As a result, in natural tissue media, the diffusion approximation to the radiative transfer equation is utilized to describe light propagation based on the premise that multiple scattering occurs in optically dense media with almost isotropic brightness [3]. The term Φ(r, t) is the fluence term, D is diffusion coefficient term, q(r, t) is the isotropic source.

$$\left[\frac{\delta}{v(\mathrm{r})\delta t} - D\nabla^2 + \mu_a(\mathrm{r})\right] \Phi(\mathrm{r},t) = q(\mathrm{r},t) \qquad (5)$$

There are two key processes for the image reconstruction in optical imaging. The first one is forward problem, during which the measurements are predicted based on the source and detector positions together with the estimated optical properties of the medium. The second key process is solving the inverse problem to determine the 3D optical characteristics (μ_a, μ_s) of the medium from the measurements. By reducing the difference between the estimated and the real measurements, a non-linear image reconstruction approach is employed to iteratively retrieve the optical properties. The DE is often employed for the forward model since it's easier to solve. The finite element method is typically utilized to solve it numerically since it allows heterogeneous solutions in irregular shape medium [3]. Our research group has developed their own forward and inverse solvers using Finite Element Method on Matlab software in both absorption and fluorescence mode [5-8]. In this work, these FEM based reconstruction algorithms have been utilized.

The inverse problem of DOT is highly ill-posed. The solution is not unique, and it is highly sensitive to noise in measurements, which yields poor quantitative accuracy and low spatial resolution in the reconstructed images. Therefore, great effort has been made to enhance DOT reconstruction by adding structural data from a high spatial resolution anatomic imaging modality [9]. Our group also adopted their FEM based algorithm to guide and constrain it with available MRI, CT, or Ultrasound anatomical data[8, 10-19].

1.2 DOT instrumentation

Three modes of operation can be adapted for DOT namely, time-domain, frequency-domain, and continuous-wave. In continuous-wave mode the measurement is only

based on the intensity of light which is used to measure the concentration or quantum yield of a fluorescent contrast agent, or absorption of the tissue[1]. In time-domain mode, the light sources create picosecond pulses, which are expanded by the tissue and detected by the detectors [1]. The light sources emit an amplitude modulated light signal in frequency mode, which is detected by detectors with reduced modulation depth, due to many scattering events in the tissue. The time-and frequency domain techniques allow recovery of the fluorescence lifetime and tissue scattering [7, 12, 14, 20, 21]

1.2.1 Continuous wave (CW)

A constant intensity light source illuminates the subject's surface in CW fluorescence tomography, and transmitted light is captured at various points on the surface surrounding the body [22-24]. CW approaches are based on determining the concentration or quantum yield of a contrast agent or tissue absorption by measuring the intensity of light. In CW method multiple source-detector pairs can be used to collect measurements of observed light. To rebuild the volumetric distribution, all the observations from the various projections are merged into an inverse mathematical model [22]. The continuous wave method is used in most commercial small animal imaging systems, because of its ease of use, availability and simplicity of instruments and hardware, and low cost.

1.2.2 Time Domain (TD)

The subject is illuminated with a short, sub nanosecond laser pulse, and a ultra-fast detector detects the arrival distribution of photons as a function of time at distinct sites in TD Diffuse optical tomography [22]. In TD Diffuse optical tomography due to scattering and absorption, a light pulse traveling through tissue is broadened and attenuated. This

broadened pulse is known as the Temporal Point Spread Function (TPSF) which is a histogram of the time it took each individual photon to travel through the tissue. This pulse of light then will stimulate a fluorophore implanted in tissue, causing it to release a fluorescence pulse with a lifespan decay unique to the fluorophore type [22]. Therefore, in TD fluorescence tomography the fluorophore and its spatial placement inside the medium determine the position, broadening, and attenuation of the TPSF histogram [22, 25]. Building TD methods necessitates the employment of very expensive and specialized equipment to measure the temporal distribution of the detected photons, , therefore TD methods are frequently perceived as the most expensive and hard to develop, although they provide the most accurate information [26],[27].

1.2.3 Frequency Domain (FD)

A light source with sine wave modulated intensity at radiofrequencies with modulation between 100–1000 MHz is used in the Frequency Domain (FD) technology. The tomographic application achieved by measuring the amplitude attenuation and phase delay of the diffusive photon waves as it propagates through tissue from multiple detection points around the tissue under investigation while the source point is varied [28].

In FD based fluorescence tomography, a fluorophore excited by intensity modulated light will emit fluorescence at the same modulation frequency, with amplitude attenuation and phase shift due to its normal fluorescence lifetime and tissue optical properties. The measured amplitude and phase delay of produced fluorescence light varies as it propagates in tissue [22]. A fast detector measures the modulated light that emerges from the surface, and a radio-frequency oscillator used to operate the diode laser provides a reference signal

for phase detection[22]. FD methods assess the amplitude and phase shift of measured transmitted or fluorescent light compared to a reference signal that can be used to determine fluorophore concentration and lifetime.

FD systems are less expensive, easier to develop, and can deliver faster scans than TD systems. The comparison of different optical tomography techniques is still a matter of discussion. CW and FD systems are very affordable, simple to create and use, and can enable rapid time scans [22]. Photon counting detectors, on the other hand, are used in TD systems are slow and expensive, but extremely sensitive. The ability to distinguish between external and endogenous fluorescence is enabled by the fluorescence lifetime, which increases the signal-to-noise ratio and thus the sensitivity. Furthermore, even if their spectra overlap, this allows multiplexing of numerous fluorescent probes with varied lifetimes. Additionally, changes in a fluorophore's fluorescence lifetime are a sensitive sign of fluorophore microenvironment variations [22, 29, 30]. It is also possible to measure the distribution of both scattering and absorption coefficients independently using TD and FD techniques, which is critical information for correct fluorophore concentration and position calculations [22]. Our group adapted FD measurement technique due to its advantages[7, 20, 21, 31-33]. But since a ICCD camera is used for the work described in this thesis, CW technique is utilized.

CHAPTER 2: Fluorescence Diffuse Optical Tomography (FDOT)

Fluorescence diffuse optical tomography is a noninvasive imaging modality provides great sensitivity, cheap cost, and safety and reliability when compared to other optical molecular imaging technologies. Due to considerable developments in fluorescent molecular probes, FDOT has become the optical molecular imaging frontier and hotspot in research and technology [34]. Fluorescence imaging has long been used to observe biological activities in living organisms, and it has greatly influenced everything from fundamental biological understanding to therapeutic application. FDOT is used in molecular imaging that captures the three-dimensional distribution of fluorescence created by a specific fluorescent material molecule within a biological tissue [34]. Advances in highly sensitive instruments have made it possible to detect fluorescence signals from whole body of small animals [35]. Unlike DOT, which measures changes in tissue absorption, FDOT measures a fluorescence signal that is unique to the exogenous fluorescent contrast agents or endogenous tissue fluorescence contrast [36].

FDOT is a straightforward extension of the DOT. The key difference is that in FDOT, tissue is illuminated by light whose wavelength matches the excitation wavelength of the fluorophore, while only the fluorescence emission light is measured on the detection sites. This can be achieved by different methods but the most common one is to utilize band-pass filter in front of the detector. The fluorescence sources deep within a medium are excited by laser light. These sources relax to their ground state and emit photons as they propagate towards the medium's surface in nanoseconds [37]. Then FDOT uses filters to separate the excitation signal from the emitted fluorescence signal when detected at the tissue surface, as

opposed to DOT, which measures the intensity variations of transmitted light through the tissue [10, 14, 37-39].

The second key difference is in the modelling part. The light propagation is modelled in two steps, first from light source to fluorophore using excitation wavelength and then from fluorophore to the detector using emission wavelength. Meanwhile the quantum efficiency, absorption and the lifetime of the fluorophore is considered in the modelling. However, the increased scattering in deep tissue makes it challenging to recover the distribution of the fluorophores and causes low spatial resolution and quantitative accuracy [35]. The FT reconstruction algorithm has been guided and constrained by structural a priori data from high-resolution imaging modalities to enhance FT quality[10, 14, 15, 20, 38]. This strategy, however, is ineffective if the fluorescent source cannot be delineated in the anatomical image or if the contrast of the fluorescent signal and the contrast of the anatomical signal are not correlated [33]. Although structural a priori information has increased FT accuracy, using functional a priori knowledge can get around some of this method's drawbacks. Direct mapping of the fluorophore distribution can be used to achieve this utilizing intriguing approaches where fluorescence imaging works in harmony with a second modality. The main component of the work described in this thesis, temperature-modulated fluorescence tomography technique, is one of the examples of such an approach[40-43].

2.1 Contrast agents utilized in FDOT

The sources of fluorescence contrast in biomedical imaging can be divided into two categories: endogenous and exogenous fluorophores [1]. Exogenous fluorophores are external sources of contrast that must be provided externally prior to imaging, whereas

endogenous fluorophores are internal sources of contrast found naturally within the body or transfected to the cells prior.

Organic dyes, proteins, and quantum dots (QDs) are the three basic types of exogenous fluorescent probes. High quantum yields and greater photostability are two advantages of QDs, however they are difficult to target [44]. Meanwhile, transfection of the green fluorescent protein GFP labeled cells with fluorescent proteins can be employed as reporter genes to provide crucial information on gene expression, protein transport, and other dynamic biochemical signals[44].

Only three fluorophores are currently FDA approved for clinical usage in the United States: ICG, fluorescein, and methylene blue (MB), all of which are organic dyes [45]. ICG is of particular importance because it is the most used NIR fluorophore in clinical imaging. Therefore, there has been a lot of interest in coupling ICG with an effective delivery mechanism to improve its photostability, quantum yield, and targeting ability. Combined with alternative approaches to deliver them to the area of interest, such as antibody labeling, many other fluorescence dyes can be utilized to target molecular processes such as VGEF, HER2, PSMA and others.

The foundation to molecular imaging is to target specific probes that report on cellular and molecular activities in the living organism. Exogenous synthetic is one approach to probe design. Exogenous probes comprise a targeting moiety for example, a receptor binding ligand, and a reporting moiety that generates a signal that may be detected by the imaging modality [37]. The reporter group must have no or only a minor effect on the probe's target contact, for instance, it must not interfere with the pharmacophore of the targeting

moiety responsible for receptor binding. Because molecular targets are often found at low concentrations, the demand for reporter principal's sensitivity has been increased [38]. Therefore, optical and fluorescence techniques are extremely suitable for such applications because they give outstanding sensitivity.

Moreover, fluorophore or fluorescent molecular probes which are also known as exogenous fluorescent contrast agents are the common design approach being used in fluorescent molecular imaging. Fluorescent probes are substances that absorb and emit light at different wavelengths. This allows FT to detect fluorescent molecular probe-labeled molecular biomarkers [37]. Therefore, it can be said that the sensitivity of fluorescence imaging is determined by the probe specificity [46].

There are a few things to think about while selecting a fluorescent molecular probe. The probe must be biologically stable in vivo, be able to overcome biological delivery hurdles, and collect large volumes of data. The probes should only produce contrast at the appropriate target to provide information about the location or specific characteristic of a disease [46]. Currently there are two types of medication targeting being used known as passive targeting and active targeting.

2.1.1 Passive targeting probes

The hyper-permeable tumor vasculature is used for passive medication targeting. Endothelial gaps and misaligned vascular endothelium cause leaky blood vessels, allowing carrier materials with sizes as small as a few hundred nanometers to enter the tumor interstitium [47]. Furthermore, abnormal lymphatic drainage causes extravasated nanomaterials to be retained within tumorous tissues. The Enhanced Permeability and

Retention effect, which is widely used in the nanomedicine area is created when these two pathophysiological properties are combined [47]. Therefore, only the pathophysiological features of target tissue and the prolonged circulation period of nanocarriers are used in passive drug targeting [47]. Therefore, nanoparticles can be effectively localized into the tumor microenvironment due to passive targeting.

Non-specific probes are the most widely available of the passive medication drug targeting, with commercial versions available for a wide range of wavelengths and purposes. Indocyanine green is the most widely used FDA-approved NIR optical contrast dyes in the United States (ICG). Through the enhanced permeability and retention (EPR) effect, ICG has attracted interest as a probe to explore hypervascularization for identification of solid tumors [46]. The circulating fluorescent probes produce background fluorescence in the blood, resulting in a low target to background signal ratio (SNR) for non-specific probe probes [46]. In breast cancer patients, ICG has shown promise in terms of sentinel lymph node mapping. In general, a non-specific fluorescence contrast agent like ICG can be employed as a physiological indication of malignant lesions, but its specificity is low because it relies on passive accumulation via the EPR effect.

2.1.2 Active Targeting probes

Active drug targeting, as opposed to passive drug targeting, is based on the insertion of unique recognition patterns within nanomedicine formulations [47]. Passive drug targeting is based on the pathophysiological features of target tissue and the longer circulation period of nanocarriers. Antibodies, peptides, nanobodies, sugar compounds, and aptamers are examples of commonly employed targeting ligands [47]. These compounds are

designed to bind to cell surface or matrix molecules that are abundant at the target region, which in the case of tumors usually refers to receptors that are highly over-expressed either by the cancer cells themselves or by other cancer cells [47]. Therefore, active targeting facilitates the active uptake of nanoparticles by the tumor cells themselves.

Moreover, active targeting is a popular way to increase the fluorophore's selectivity to the target spot. This has the additional benefit of increasing the contrast between malignant and healthy tissue. The specificity and sensitivity achieved are determined by the biomarker and targeted moiety used [48]. A detectable NIR fluorophore is attached to a specific targeting moiety (i.e. antibodies, antibody fragments, proteins, peptides, etc.) that has a high affinity and binds precisely to a certain receptor in this approach [49]. This allows the fluorescent probe to recognize and bind to a specific molecular target, enhancing contrast and retention time by keeping the fluorophore in the targeted location for a long time.

2.1.3 Probes with smart activation

Smart or activatable molecular probes are an alternate technique for improving specificity and signal to background noise ratio (SNR) by lowering background signal and enhancing target signal [50]. Smart or activatable molecular probes can reduce background noise while increasing target signal. These probes work by changing the quantum yield of fluorescent dyes in a regulated manner. Only until the probes have been precisely activated by a target, they do not produce a signal. Because activated probes are relatively undetected in their initial injected state, they can achieve high target-to-background signals [51], [52]. Conformational changes caused by environmental parameters such as pH, oxygenation, and

temperature can also activate probes, which can provide vital functional information about the tumor microenvironment [53-57]. Temperature sensitive polymers like polyNIPAM derivatives and poloxamers like Pluronics can be used to achieve thermal activation. Activation occurs when paired with a polarity-sensitive fluorescent dye like ICG or benzofurazan, which emits high fluorescence in hydrophobic environments [58].

Many reversible activated probes can provide functional information on the tumor microenvironment and hence have the potential to provide real-time monitoring [50]. Activatable probes can also be targeted, enhancing their specificity and sensitivity when it comes to disease detection.

2.2 Modeling of light propagation and image reconstruction in FDOT

Besides light scattering and absorption, the fluorescence process is needed to be considered to be able to model the light propagation for FDOT. Since fluorophores act as an additional source of illumination, the mathematical modeling of FDOT is different then conventional DOT, which will be explained in detail in this chapter.

In terms of the electronic and vibrational energy levels, the Jablonski diagram represents the link between absorption and photoluminescence processes (fluorescence and phosphorescence) [59]. Luminescence is the ability of some atoms and molecules to absorb light of a specific wavelength and then emit light of a different wavelength after a brief period. The time it takes for each transition to occur refers to the probability of each process occurring [59].

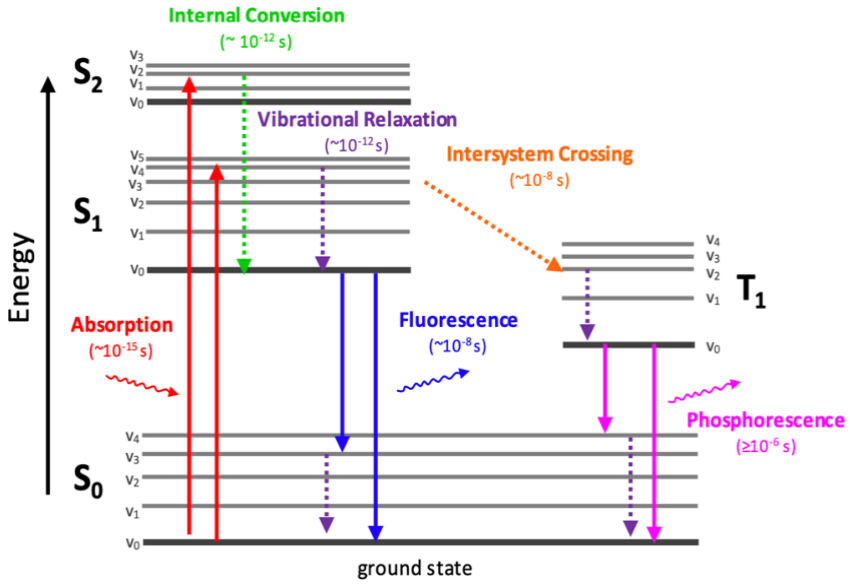

Figure 2.1: Represents the Jablonski Diagram. A fluorophore's typical paths after being excited by a single photon are depicted as the (ground, first excited, and second excited) singlet electronic states that are represented by S0, S1, and S2. The vibrational energy levels are represented.

As shown in Figure 2.1 The absorption of a photon is the first (and fastest) stage in the luminescence process. A molecule or an atom can absorb a photon of a specific energy in this process. This energy is transferred to an electron, enabling it to transition from a lower energy level to an excited singlet electronic state (i.e., S0→S1)[60]. Molecules only absorb wavelengths of light that match the energy difference between their two different energy levels. Therefore, the energy of the absorbed photon corresponds to the gap between excited and non-excited states.

Once an electron has reached its excited state, it can undergo several processes to return to its more stable ground state (S0). As illustrated in Figure 2.1 the relaxation to the initial excited state's (S1) lowest vibrational energy level is the most likely occurrence [60]. This is commonly accomplished through vibrational relaxation, a nonradiative process in which the electron decays to lower vibrational levels while remaining in the same electronic

state. Another process is the occurrence of the internal conversion which happens when an electron in a different electronic state shifts to a lower vibrational energy level. Both processes are nonradiative, as energy is normally wasted as heat, and they take place in fractions of a second [60].

Fluorescence emission is another way of losing energy by the electron. When a photon decays from the first electrically excited state to the ground state, (S1→S0), fluorescence emission occurs [60]. In comparison to vibrational relaxation and internal conversion, this radiative process is relatively slow ($\sim 10^{-8}$ s) [61]. Therefore, fluorescence emission will most frequently occur between the first excited electron state and the ground state, as internal conversion becomes less efficient as the energy difference widens.

2.1.2 Stokes Shift

Fluorescent materials absorb higher energy and emit lower energy photons. For example. the FDA approved fluorophore, indocyanine green, has a peak excitation and emission wavelengths of 785 nm and 830 nm, respectively. As illustrated in Figure 2.2, the emitted fluorescence light has a lower energy and longer wavelength, known as the Stokes shift. We use this shift in fluorescence imaging to isolate the emission light from the excitation signal using optical bandpass filters as shown in Figure 2.2 [62, 63].

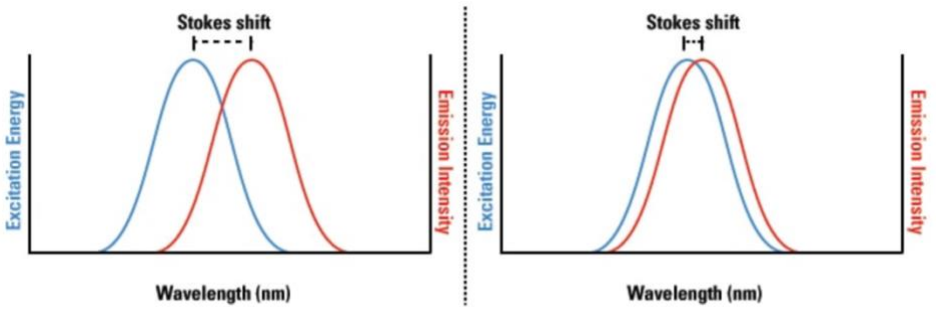

Figure 2.2: Stokes shift of a fluorophore's excitation and emission spectra. fluorophores with larger Stokes shifts (left) show a clear contrast between excitation and emission light in a sample, whereas fluorophores with smaller Stokes shifts (right) have a higher background signal.

2.1.3 Quantum Yield

The efficiency with which light is absorbed and converted to fluorescence is referred to as quantum yield or quantum efficiency. The fluorophore fluorescein and the green fluorescent protein (GFP) have large quantum yields of ~0.9 and ~0.8 respectively [60], whereas ICG has a quantum yield of 0.016 [64]. Eq.6 is the quantum yield, which is the proportion of photons emitted $I_{emitted}$ *to* photons absorbed $I_{absorbed}$:

$$\eta = \frac{number\ of\ photons\ emitted}{number\ of\ photons\ absorbed} = \frac{I_{emitted}}{I_{absorbed}} \quad (6)$$

2.1.4 Fluorescence Lifetime

The average duration a molecule stays in an excited state before emitting a photon is referred to as the fluorescence lifetime. Because fluorescence is a spontaneous emission, the electron usually stays in the fluorescence state for several nanoseconds before decaying to the ground state. Fluorescence lifetime can therefore be used to investigate changes in the fluorophore microenvironment. Furthermore, even if their emission and excitation

spectrum overlap, lifetime measurements can be utilized to differentiate different sources of fluorescence [22].

2.1.5 Photobleaching

Photobleaching is the loss of fluorescence induced by the degradation of the fluorophore caused by light exposure. The number of excitation and emission cycles is determined by the fluorophore's molecular structure and its surrounding environment. Photobleaching results in a permanent loss of fluorescence signal, as opposed to quenching, which is a reversible loss caused by noncovalent interactions between the fluorophore and the surrounding molecular environment [60]. However, not all photobleaching is undesirable, as evidenced using fluorescence recovery after photobleaching (FRAP) to evaluate fluorophore diffusion rates [65]. When compared to the excited singlet state, the fluorophore spends more time in the excited triplet state, giving it more time to interact with other molecules and undertake chemical reactions in the environment. Fluorophore molecules in a target location are purposefully bleached in this method to detect the diffusion of new fluorophore molecules into the target region.

2.1.6 Mathematical modeling of light propagation in FDOT

It is possible to think of FDOT forward and inverse problems as an extension of DOT. Due to the presence of fluorophores in the medium, FDOT has an additional source term. It is anticipated that the excitation and emission wavelengths will have different diffusion equation solutions. Modeling the propagation of light from the external source on the tissue's surface to the internal fluorophore inside the medium is the first stage. Second, a model is

created to estimate how fluorescent light from the internal fluorophore propagates to the detectors at the tissue boundary [66].

$$\begin{cases} \nabla.(-D(\mathrm{r})\nabla\mu_{\chi}(\mathrm{r},\mathrm{r}_s)) + \mu_a(\mathrm{r})\mu_{\chi}(\mathrm{r},\mathrm{r}_s) = q(\mathrm{r}_s) \\ \nabla.(-D(\mathrm{r}')\nabla\mu_m(\mathrm{r}',\mathrm{r},\mathrm{r}_s) = \beta(\mathrm{r})\mu_{\chi}(\mathrm{r},\mathrm{r}_s) \end{cases} \quad (7)$$

The first equation simply models the light propagation for the excitation light (subscript $_x$); and describes the excitation photon density from the source point s_a, to the position of the fluorophore r in the diffusing medium. Given the inherent characteristics of the fluorophore and the excitation photon density, which was obtained from the first equation, the second equation predicts the light propagation of the fluorescent light (subscript $_m$) released by the fluorescent source at point r'. The diffusion coefficient is denoted by the letter D, while the total absorption in the volume is represented by the coefficient μ_a. The conversion rate of excitation light into fluorescence light at a point r is determined by the intrinsic properties of the fluorochromes, such as the quantum yield and local concentration. This parameter, βr, is part of the fluorescence source term[66].

2.1.7 FDOT image reconstruction

The FDOT inverse problem is resolved using a least-square minimization approach. This method is the same as the one employed in DOT with the exception of the fact that we are currently minimizing the difference between the real and simulated measurements, using the coupled diffusion equation to get the spatially resolved fluorophore absorption coefficient μ_a and lifetime.

The fluorophore's size, position, and concentration have a significant impact on the accuracy of the recovered fluorescence parameters. Like DOT, FDOT suffers from poor spatial resolution because of the significant light scattering in tissue. As a result, to improve the FDOT reconstruction, FT has also been merged with other high spatial resolution imaging modalities by adding anatomical information as structural a priori knowledge. In this approach, a specific area in the FEM mesh delineated by the high-resolution imaging modality is assigned with initial fluorescence distribution and treated differently during the iterative process [33, 67]

2.2 Limitations of the FDOT

FDOT is a new biomedical imaging technique that can be used to locate and quantify fluorescent molecules that are deeply embedded in tissues. However, its potential is limited by its lack of spatial resolution and poor quantitative accuracy [68]. Spatial resolution is a fundamental problem for both DOT and FDOT, due to ill-posed and underdetermined inverse problem [1, 69]. Hence, additional structural information has been used to guide and constrain the FDOT inverse problem and improve the reconstructed images. This multimodality approach also allows perfect co-registration of FDOT images with anatomic images obtain by other modalities such as MRI, X-ray, or ultrasound. For instance, when FDOT is used in conjunction with other structural imaging modalities, it can improve lesion localization and assessment of functional tissue characteristics which has shown promise in the diagnosis and prognosis of breast cancer [69]. As of now, FDOT has been effectively integrated with X-ray mammography, ultrasound, and MRI [70]. Multimodality imaging is

especially useful in the case of breast cancer since the compressibility of breast tissue makes co-registration with nonconcurrent data challenging, necessitating complex deformation algorithms and assumptions [70]. Despite this progress, unfortunately FDOT have not been translated to the clinical arena since multi-modality approach has its own challenges.

CHAPTER 3: Temperature Modulated Fluorescence Tomography (TM-FT)

As previously mentioned, the FDOT is the method of choice for whole-body fluorescence imaging of small animals due to its superior sensitivity. However, the fundamental obstacle to its clinical translation has been its subpar spatial resolution, despite its higher sensitivity. This restriction is mostly caused by the high optical photon scattering in biological tissue and the insufficient surface measurements, which result in an underdetermined and ill-posed inverse problem. It has been proven that combining FDOT with standard anatomical imaging modalities, including X-ray CT, MRI, or ultrasound, can enhance FDOT accuracy greatly. However, co-registration of images obtained at different settings is one of the major challenges for multi-modality imaging [2, 4, 46, 59, 60, 71, 72]. Another drawback of multi-modality imaging is that the structural imaging modalities cannot quantify fluorescence. As a result, when the anatomical images are co-registered with the FDOT, a major assumption must be made that fluorescence contrast is supposed to correlate with anatomical contrast [69]. However, errors can occur when the structural limits provided by the anatomical imaging modality do not perfectly correlate with the true fluorescence distribution.

Dr. Gulsen's team developed "temperature-modulated fluorescence tomography" (TM-FT) at UCI to alleviate these problems. By combining two modalities, high intensity focused ultrasound (HIFU) and fluorescence tomography, TM-FT delivers high-resolution images without sacrificing the high sensitivity of fluorescence-based detection[73]. Unlike conventional multi-modality imaging systems, where anatomic imaging modalities operate

independently, focused ultrasound and fluorescence tomography work together in harmony here making TMFT a true multimodality approach. In this approach, both modalities interact to produce images that neither could produce alone. The sensitivity of this technology is based on the responsiveness of the "ThermoDots," which are activatable thermo-reversible fluorescent probes. In TM-FT, high-intensity, low-power, focused ultrasound (HIFU) waves are employed to stimulate the medium. The primary advantage of HIFU is the ability to modulate the medium temperature about four degrees Celsius over a very short time around one second with a very high spatial precision of approximately one millimeter as shown in Figure 3.1b [73]. As a result, only when thermodots are present within the focal zone the intensity and lifespan of emitted fluorescence light have noticeable change as seen in Figure 3.1C [73]. Figure 3.1a represents the 3D schematic of the HIFU scan over the phantom medium.

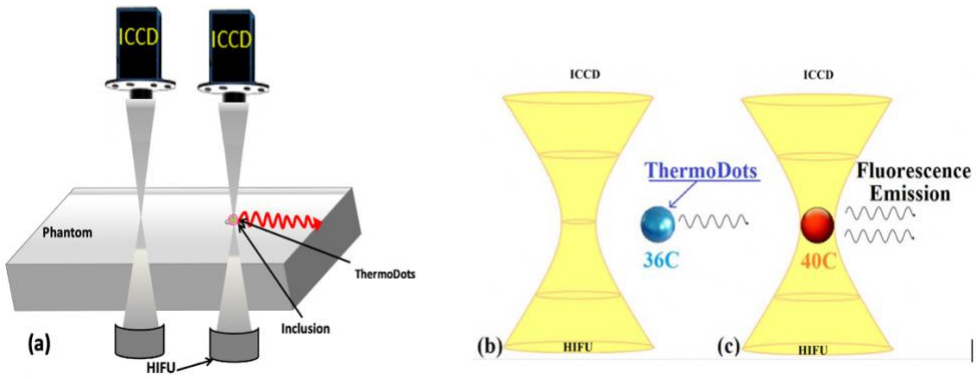

Figure 3.1: a) 3D Schematic of HIFU scan b) A localized temperature increases of 4°C occurs on the focus spot of 1mm during the HIFU scan. c) When ThermoDots are present within the HIFU focal zone, the temperature rises, changing the quantum efficiency and hence the fluorescence emission light intensity [73].

TM-FT enables high-resolution fluorescence imaging by scanning a focused ultrasonic column over the medium and detecting variations in the released fluorescence signal. Furthermore, the HIFU transducer can produce hot spots up to a depth of 6cm. Because the spatial resolution of HIFU is mostly governed by the spot size, even thick tissue can attain great spatial resolution ~1.33mm [33]. The temperature-sensitive fluorescence probes are first located using focused ultrasound via TM-FT. Following that, this a priori information is used to increase the performance of the inverse solver for traditional FDOT, resulting in quantitatively reliable fluorophore concentration maps [73]. As a result, TM-FT uses the *a priori* binary location information provided by the temperature modulation of the ThermoDots (i.e., utilizing them as binary ON/OFF switches) to provide fluorescence images with substantially higher spatial resolution than standard FDOT [73].

The ThermoDots' responsiveness is critical to the TM-FT sensitivity. ThermoDots are temperature-sensitive fluorescence contrast agents made with ICG-loaded pluronic nanocapsules [74].The thermo-responsiveness of the ThermoDots is based on the pluronic polymer micelles, which have temperature-dependent hydrophobic/hydrophilic characteristic. A hydration layer surrounds Pulornic F-127 molecules at low temperatures. However, the hydrophilic chains of the copolymer become dissolved as the temperature rises [33]. This effect promotes hydrophobic contacts between the polyoxypropylene domains, resulting in the development of gels. The gel is assumed to be micellar in composition. At low temperatures, a liquid micellar phase is stable, but as the temperature rises, it converts into a cubic structure [75]. A phase of hexagonal-packed cylinders forms at higher temperatures. Therefore, it can be said the thermo-responsiveness of the ThermoDots is based on the temperature-dependency of the Pluronic polymer micelles

caused by their hydrophobic/hydrophilic characteristic [75]. Because an increase in temperature causes a change in the solvent polarity, ThermoDots can operate as a fluorescent switch, resulting in an ICG fluorescence signal and lifespan change. Because these contrast agents are temperature dependent, temperature modulation can be used to solve the spatial resolution restriction of conventional FDOT.

Moreover, the HIFU creates a hot spot as it scans across the medium, raising the temperature of this small area by several degrees. The fluorescence quantum efficiency increases when temperature-sensitive fluorescence agents are present within this focal zone due to the raised local temperature. This temperature modulation enables for individual fluorescence measurements for each pixel in a region of interest (ROI), which isn't possible with traditional FDOT.

Therefore, TM-FT allows fluorescence imaging with high spatial resolution by scanning focused ultrasound columns over the medium. In this approach, first a conventional low resolution FDOT image is reconstructed to define a region of interest (ROI) around the target. Then, a focused ultrasound line is scanned over this ROI while monitoring the change in the fluorescence signal. This procedure localizes the thermoDots at focused ultrasound resolution (~1.33 mm) and creates a binary map of the fluorophore distribution. Finally, the boundary of the fluorescent target outlined by this procedure is used as a priori information to recover quantitatively accurate concentration and lifetime images using the conventional FDOT data.

3.1 Development of ThermoDots

ThermoDots are temperature-sensitive fluorescence contrast agents made with ICG-loaded Pluronic nano capsules [74]. The two main components of these ThermoDots are fluorescent dye Indocyanine Green particles and Pluronic F-127 powder.

3.1.1 Fluorescent dye Indocyanine Green (ICG)

As aforementioned the only FDA-approved fluorophore for medical diagnostics is Indocyanine Green (ICG). Because of its lipophilic polycyclic portions and hydrophilic sulfate groups, ICG has amphiphilic characteristics [76]. It works in the near-infrared range (700-900 nm), which has several advantages over visible fluorophores [77]. Because ICG binds strongly to plasma proteins in the blood, it can be utilized to examine tumor vascular permeability. When compared to healthy or benign tissue, malignant tumors had higher absorption due to ICG buildup and slower rate constants (slower uptake, delayed peak, and slower outflow) [78].

ICG delivery, accumulation, and retention in the tumor are critical, however due to its thermal, photo-degradation, and aqueous instability, its applications are limited [79]. ICG is amphiphilic, and large concentrations cause it to aggregate and quench, resulting in a decreased fluorescence quantum yield. The concentration-dependent absorption characteristics of ICG are not always linear. Higher temperatures, as well as pH, play a role in the degradation of ICG [79].

3.1.2 Pluronic F-127

The thermo-sensitive micelles composed of Pluronic polymers are the second primary component of the ThermoDots. Pluronic F-127 is a nonionic triblock copolymer that consists of two polyethylene oxide blocks connected by a poly propylene oxide (PPO) block. PEO is the most water-soluble polymer and is very hydrophilic [80]. PPO, on the other hand, is hydrophobic at high temperatures but water soluble at low concentrations [81]. Therefore, at room temperature PPO is very hydrophobic and does not dissolve in water. amphiphilic nature of Pluronic leads to the spherical micelle formation with a hydrophobic PPO core and a hydrophilic PEO shell [82]. Therefore, Micelle formation is dependent on concentration of the Pluronic as well as temperature since PPO dissolves in water at low temperatures. The temperature and concentration at which micelles are formed are known as the critical micelle formation temperature (CMT) and micelle formation concentration (CMC) respectively.

Functionalization of polymeric nanoparticles allows for active targeting and increased circulation time [83]. The change in hydrophobicity/hydrophilicity property as the temperature changes causes the polymer to behave thermally responsively. This change in fluorescence is reversible and is based on the activable thermos reversible NIR fluorescent nanoprobes called ThermoDots.

3.1.3 Synthesis of ThermoDots

ICG is encapsulated in Pluronic polymeric micelles to make the ThermoDots. Figure 3.2 shows how ICG is encapsulated into micelles using a solvent evaporation approach. First the Pluronic solution is made using DI water and Pluronic F-127 powder. Secondly,

ICG complex is formed using Tetraoctylammonium bromide (TOAB) and ICG powder mixed in chloroform. Then 200ul of ICG complex is added dropwise with micropipette to the 10 ml of the aqueous Pluronic micelle solution. The solution is then evaporated to form Pluronic-ICG nano capsules.

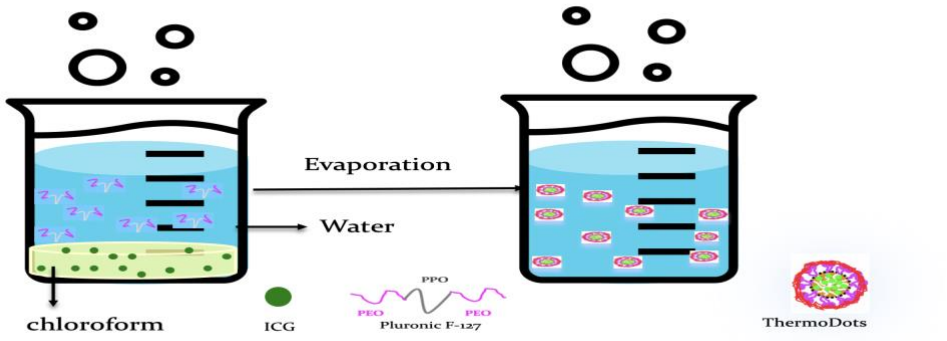

Figure 3.2: The process of engineering ICG enclosed Pluronic micelles using a solvent evaporation process.

After evaporation process the Pluronic-ICG solution is filtered using centrifuge, and washed with deionized water to remove free ICG particles from the solution [46]. To characterize the ThermoDots solution and identify their activation temperature range, a tiny sample is used. The ThermoDots are then stored in the dark and kept at 4°C. They are maintained in glass vials coated in aluminum foil to prevent light exposure from the outdoors.

3.2 Fiber-based TM-FT Instrumentation

There are two aspects to the TMFT system: FDOT and focused ultrasound. The object under examination is illuminated by a 785 nm laser diode for FDOT. The laser light is sent to one of eight source optical fibers via a fiber optic switch. The laser-diode is simultaneously

modulated with RF (100 MHz) while the amplitude of the detected signal is measured using a network analyzer (Agilent Technologies, Palo Alto, CA). One of eight optical fibers collected the transmitted photons and transported them through a sequence of lenses (Newport Corporation, CA) and band-pass filters (830 nm, MK Photonics, Albuquerque, NM) that collimated, filtered out excitation light, and focused the photons to the detector. The fluorescence signal is detected using a photomultiplier tube (PMT) (R7400U-20, Hamamatsu, Japan). Before being captured by the network analyzer, the signal is amplified by an RF amplifier. Figure 3.3 illustrated the fiber-based TM-FT system.

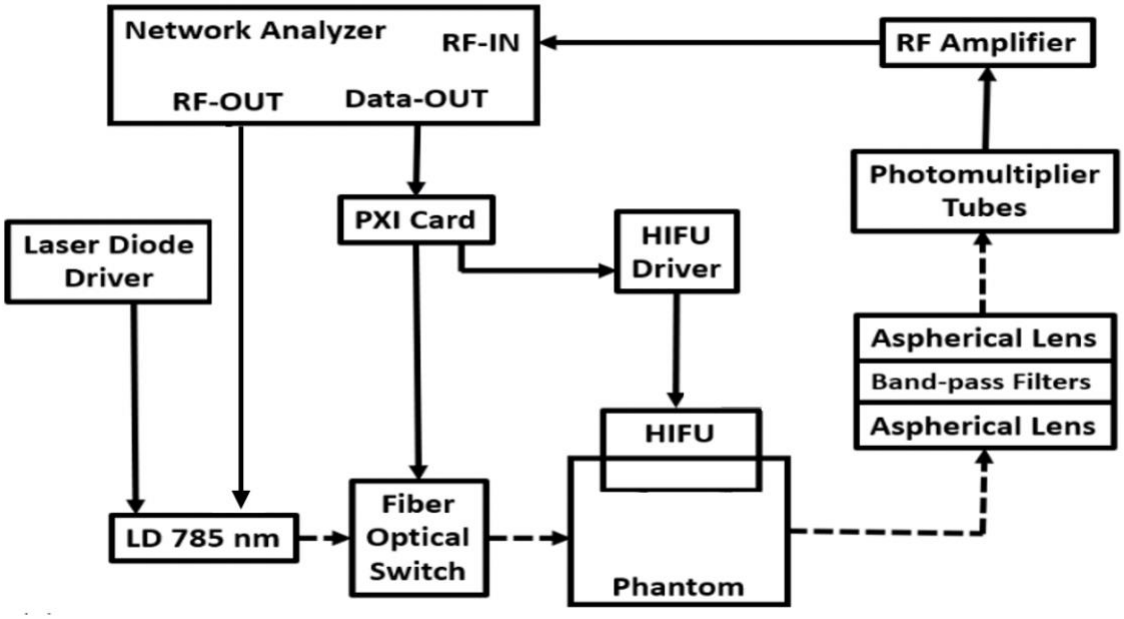

Figure 3.3: Fiber based TM-FT system diagram.

The HIFU is the second component of the TMFT system. Focused ultrasound is a technique that uses ultrasonic waves to transfer energy through a medium and induce a variety of thermal or mechanical biological effects at a certain depth and location [84, 85].

This method delivers localized heating by focusing acoustic waves to create a zone of extreme pressure and heat known as a “hotspot”. This enables for localized heating with minimal damage on adjacent tissue [84, 85]. In TM-FT system HIFU is used to modify the temperature of the medium at a focused hotspot (~1.33 mm) to map the distribution of temperature-sensitive fluorescence contrast agents and retrieve functional a priorities non-invasive method has shown improvements in tumor ablation, targeted medication delivery, and thrombolysis. The TM- FT is safe since it uses low-power focused ultrasound to heat the tissue a few degrees (max temp 42°C) over a short period of time (less than 2 seconds). To focus the acoustic waves at a fixed location, a spherically curved transducer (H-102 transducer, MR-compatible, Sonic Concepts, Inc., WA, USA) is employed. This self-focusing approach is the simplest, least expensive, and typically most precise method compared to the other types of focusing methods [85].

The cylindrical focus zone of this HIFU transducer is 1.33 mm in diameter and 10 mm in height, and it is positioned at a depth of 60 mm. The HIFU is installed on a computerized translational stage, allowing it to be scanned in all three orthogonal directions [71]. In the fiber-based TM-FT version, the HIFU is scanned from the top side of the phantom.

3.2.1 TMFT fiber-based data acquisition

To collect full tomographic measurements for traditional FDOT, eight sources and detectors in transmission arrangement are used, as shown in Fig. 3.4a. This setup generates 64 measurements and permits the reconstruction of 3D fluorescence concentration map [86]. To test the performance of the system, a 3 mm diameter fluorescent target is positioned

20 mm from each boundary in the middle of the synthetic phantom. Fig. 3.4b displays the reconstructed conventional FDOT fluorescence map.

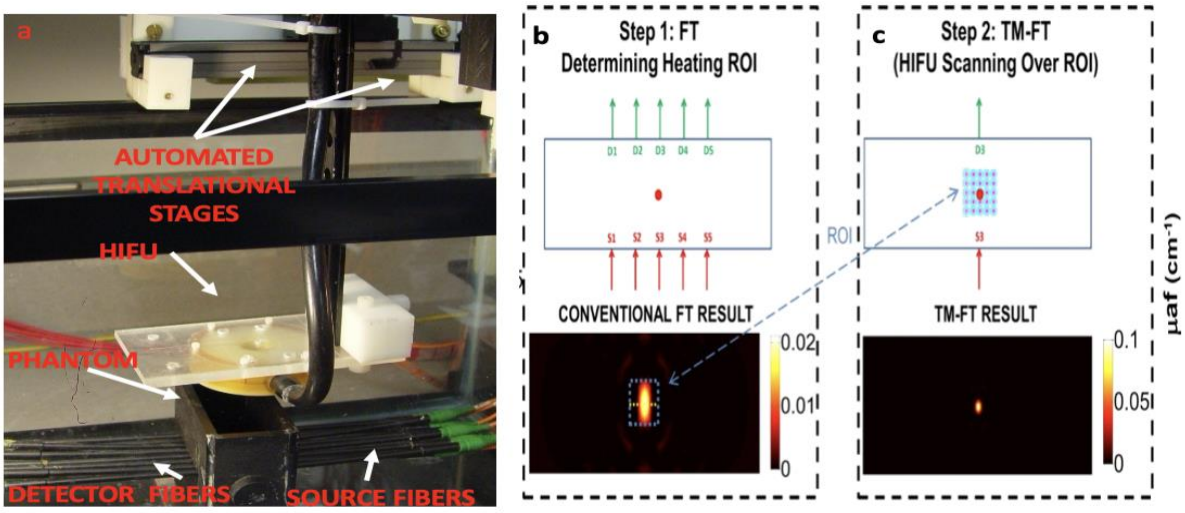

Figure 3.4: a) Is the illustration of fiber-based TM-FT. b) illustration of how to determine a heating ROI and the conventional FDOT result. C) Represents HIFU scanning over ROI using TM-FT system and TM-FT result.

The HIFU beam is then scanned over the ROI once it has been determined using the low-resolution conventional FDOT images that are recovered in the preceding stage Figure 3.4c. The intensity of the fluorescence emission, consequently the measured signal changes significantly due to changes in quantum efficiency, only when the temperature-sensitive contrast agent is present inside the focal spot. Thus, a binary mask that provides a precise description of the contrast agent distribution is obtained. Here, the spot size of HIFU (1.33 mm) is closely correlated with the resolution of TM-FT. Obtained binary mask already represents a high-resolution fluorescence image even without any reconstruction process. However, a final TM-FT reconstruction process is required to achieve a quantitatively

accurate contrast agent concentration map. The real μaf of the fluorophore is set to 1 (1/cm) while the mean recovered μaf for this inclusion is 0.014 and 0.094 for the conventional FDOT and TM-FT, respectively. The results show that the error in the recovered fluorophore μaf decreases from 86% down to 6%, more than 10-fold when TM-FT is utilized. This is actually directly related to the resolution capability of the TM-FT. The size of the inclusion recovered by the conventional FDOT is 4.3mm & 10.4mm in x- and y-axis, respectively. However, it reduces to 3.0mm & 4.2mm in x- and y- axis, respectively, when TM-FT is utilized. This validation study illustrates the superior resolution and quantitative accuracy of the TM-FT. Despite its high performance, this fiber-based TM-FT system has its own challenges. That is the main reason behind the motivation of the development of the ICCD -based TM-FT system as described in the next chapter.

CHAPTER 4: An ICCD Based TM-FT System

This fiber-based scheme presented several limitations that hampered the translation of TM-FT to *in vivo* imaging. Mainly, the animal had to be immersed in an optical index matching fluid and the detection sites were limited by the number of detection fibers. Therefore, this design is unsuitable for *in vivo* imaging. To alleviate these concerns, the focus in this thesis is to develop an ICCD camera-based TM-FT small animal system. The new prototype offers greater sensitivity in addition to being more suitable and high throughput for *in vivo* preclinical studies.

In this version an intensified CCD camera replaces the fiber optics detection system that utilizes PMTs as point detectors. The camera is positioned on top of the animal, and the HIFU is placed underneath to do scanning from the animal's bottom, as shown in Figure 4.1. Therefore, the animal does not have to be fully submerged into an optical matching fluid for *in vivo studies,* since it is positioned on an ultrasound & light transparent membrane. Moreover, this approach offers a uniform detection sensitivity over the entire animal using this acquisition approach versus the limited detection due to limited numbers of optical fiber detectors in the fiber-based system.

3.2.2 ICCD based TM-FT instrumentation

As aforementioned this new system relies on intensified CCD camera for real time data collection. The intensified camera used in the new TM-FT system is made up of a high-performance CCD camera and an image intensifier positioned in front of it. The image intensifier amplifies the input light first. The intensified image is then projected onto a CCD sensor through a coupling tapered fiber bundle from the intensifier's phosphor screen. As a result, the ICCD camera amplifies incoming light, providing a light sensitivity well below the CCD sensor's thermal noise limit [87]. Hence, ICCD camera enhances the signals and reduces the overall imaging time. Moreover, a filter wheel is employed between the ICCD camera and its lens to quickly transition between DOT and FDOT measurement modes. Figure 4.1 shows the schematic and the picture of this ICCD-based TMFT system. To stimulate the ThermoDots, a 785 nm laser is utilized. A second box next to the system houses the laser and its driver. An optical fiber is used to transmit the laser's output to the TMFT system. They

are moved in tandem on a predetermined grid by a computer-controlled translation stage, and ICCD images are taken both with and without the HIFU beam at each location.

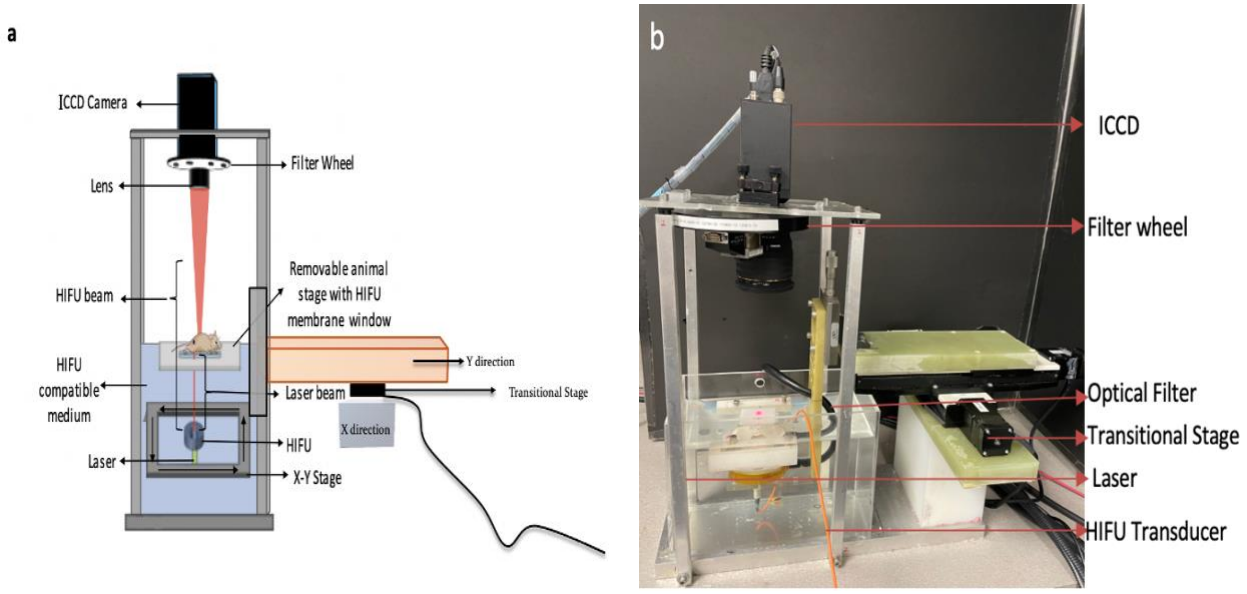

Figure 4.1: a) is the schematic of the ICCD- based TM-FT, and b) is the picture of the ICCD-Based TM-FT prototype system.

4.1 Experimental procedure

4.1.1 Characterization of ThermoDots

A frequency domain fluorescence system is built to characterize the ThermoDots. At the beginning the Thermodots are first characterized quickly to evaluate their temperature responsiveness. Afterwards, the ThermoDots sample is heated and cooled in a controlled manner utilizing two thermoelectric coolers for this operation (TEC). The temperature of the ThermoDots solution sample is recorded together with the change in fluorescence intensity. Figure 4.2 shows the diagram of the customized temperature characterization system. A

3mm diameter, 8 cm long, NMR tube glass is used to hold the ThemoDots during characterization. Figure 4.2 shows two detector fibers arranged at opposite sides of the copper plate, which is used to hold the NMR tube in place. The excitation source fiber is inserted to the hole prepared on the copper plate orthogonal to the detector fibers. To monitor the sample temperature, a fiber-optic temperature sensor is put inside the sample tube. Two TECs beneath the copper holder controls the temperature of the copper plate, hence the sample. A power supply is used to control the supply of the current with a maximum of 3 A of current being supplied to the TECs.

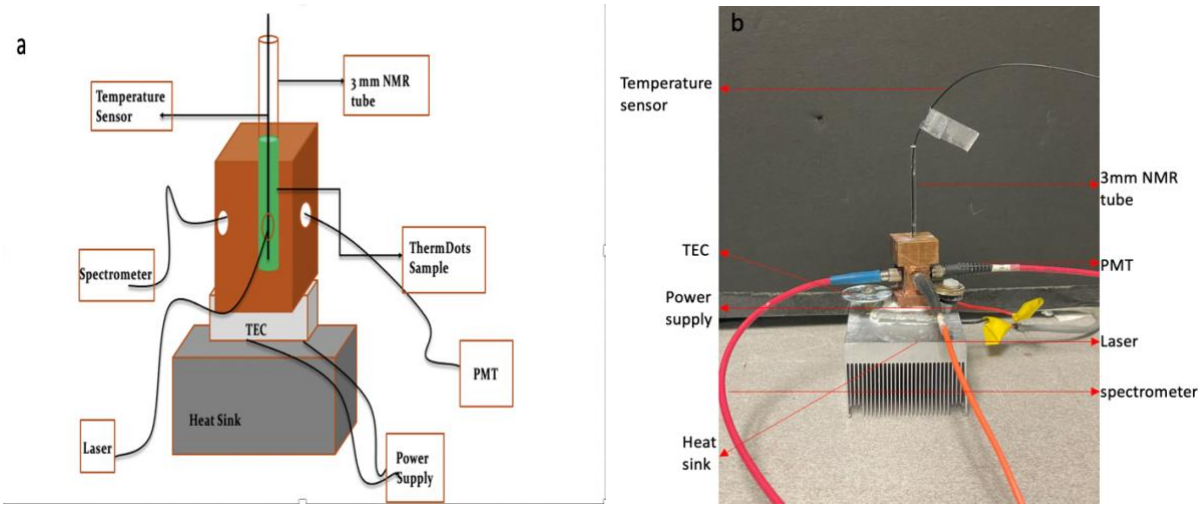

Figure 4.2: a) The schematic and b) the actual prototype of the agent holder system used in characterization process.

For fluorescence excitation, a 785-nm laser diode (300 mW), Thorlabs, Newton, New Jersey, USA) is employed, with a fiber optic switch used to turn the laser light on and off. For fluorescent light detection, a photomultiplier tube (PMT) and spectrometer (USB2000, Ocean Optics, Florida, USA) were employed simultaneously. A network analyzer (Agilent Technologies, Palo Alto, California) generates a 100 MHz RF signal and evaluates the

amplitude and phase of the observed fluorescence signal. The sample is heated gently (1 degree/minute) until the fluorescence intensity plateaus to define the thermo-responsiveness of the ThermoDots. This process allows us to evaluate the fluorescence quantum efficiency of ThermoDots, which is calculated by variation in the amplitude of the emitted signal intensities. The activatable temperature range of TermoDots made using pluronic F-127 polymers is between 17-23 °C. Therefore, data is acquired a minimum of five degrees above and below the activatable temperature range of ThermoDots. Each PMT fluorescence measurement is then averaged three times for better accuracy. The spectrometer also has a 200-millisecond integration time and averaging of two is used to reduce the noise. Figure 4.3 illustrates the diagram of fiber-based frequency domain system used to characterize ThermoDots.

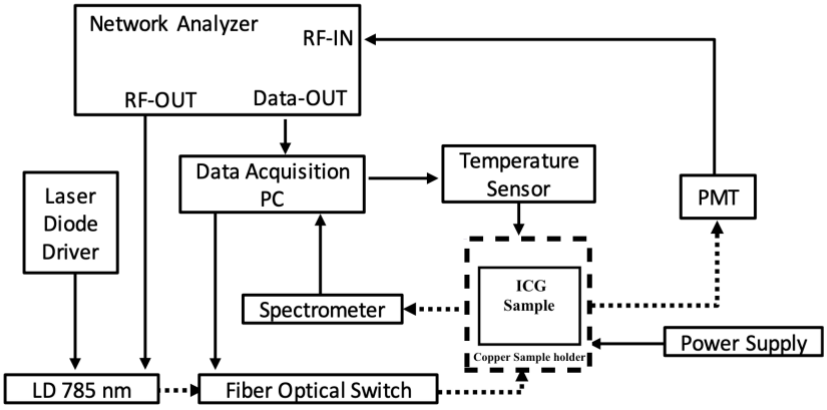

Figure 4.3: This diagram illustrates the frequency domain system used to characterize the temperature dependency of ThermoDots.

Figure 4.4 shows the fluorescence signal as a function of local temperature using a ThermoDots formulation of 3% Pluronic F-127 micelle/20 M. The fluorescence signal

amplitude increases roughly 31 dBm as the temperature is raised by merely 4°C from 17-23°C, showing an increased ICG fluorescence quantum yield. These findings correlate to the previous findings that the interior of the micelles becomes more hydrophobic as the temperature rises, resulting in a boost in fluorescence quantum efficiency and longevity [88, 89].

Figure 4.4: Illustration of the ThermoDots fluorescence emission temperature dependency designed for the phantom study in the range of 17-23 °C.

Outside of the activation temperature range 17-23°C, the signal plateaus because the micelle core's hydrophobicity remains unchanged. Furthermore, the fluorescence response of ThermoDots to local temperature in its activation range is reversible. The encapsulated ICG response to the changing hydrophobic/hydrophilic environment in the Pluronic micelle core with temperature causes this reversible shift.

4.1.2 ICCD based TM-FT phantom studies

Tissue simulating phantoms are used to evaluate, analyze, and fine-tune the performance of an imaging device without sacrificing live subjects. Therefore, phantoms play a crucial role for design, testing, and validation of biomedical imaging systems since they closely mimic biological tissues characteristics [90]. Furthermore, they are less complex and yield more consistent findings than live biological tissue and hence, can be used as calibration standards.

Solid, liquid, and agarose gel phantoms are the three forms of tissue-mimicking phantoms used in optical imaging. The purpose is to match the optical properties of the phantom with biological tissue, which is done by adding absorbers, scatterers, and fluorophores to closely match the desirable tissue type [90]. However, the incorporation of focused ultrasound in the TMFT system, necessitates simulating the same thermal and mechanical properties of biological tissue as well as propagation of ultrasound waves. As a result, TM-FT phantoms are predominantly made from liquid and agarose gel phantoms.

Clinical grade Intralipid (Intralipid® 0.5%, Fresenius Kabi, Uppsala, Sweden) is employed as an optical scatterer in phantom investigations because it is affordable, widely available, and biocompatible. Moreover, Indian ink (Winsor and Newton, UK) is used commercially as an optical absorber. Agarose gel phantoms created in this experiment are made using agarose powder (OmniPur® Agarose Gel, EM Science, Gibbstown, NJ) since it allows to vary the phantom's viscosity and can be used to tune the phantom's mechanical and thermal properties. The addition of agarose powder necessitates the heating of the phantom as well as extra cooling and setting time. For the purpose of this experiment the

agarose gel is mixed with intralipid (0.5%) and India ink to adjust the phantoms' absorption and reduced scattering coefficients to 0.01 mm^{-1} and 0.8 mm^{-1}, respectively. Since the agarose gel phantoms lack a definite shape, they necessitate the usage of a mold. Unfortunately, due to the small inclusion size in this thesis, the fluorescent inclusion cannot be created from agarose powder. To hold the liquid solution, the ThermoDot sample is placed into NMR tubes buried vertically inside the phantom as shown in Figure 4.5 The bottom center of the phantoms is designated as the origin of the spatial coordinates. A 3-mm-diameter and 10-mm-high cylindrical glass tube is first inserted at the center of the first phantom along its z-axis to produce a zone with ThermoDots accumulation within the phantoms. Figure 4.5b displays the ICCD room light image over the imaging interface's field of view. The dimensions of the agarose phantom used for this research study is placed in a rectangular shaped 5mm×3mm size mold. Moreover, the ICCD camera is placed on top of the phantom surface right in the center. The laser light collimator is placed below the NMR tube holding the ThermoDots solution exactly in the center for best excitation, while the ICCD camera is mounted right on top of the phantom. Figure 4.5a represents the 3D schematic of phantom placement with respect to the ICCD camera and HIFU location. Figure 4.5b shows a top view of phantom, which the HIFU is located underneath of the phantom and the upper surface of the phantom is perched on top of the transparent membrane. Figure 4.5c, d shows the fluorescence images that the ICCD took while the HIFU hot spot is directly beneath the glass tube housing the ThermoDots. To show how local heating affects the response of ThermoDots, the power of the HIFU is adjusted to raise the tube's temperature by 1^{o}C and then 2^{o}C, respectively. When the local temperature raised due to the HIFU, the ThermoDots

became visible in the images. As predicted, the fluorescence signal of the ThermoDots increases proportionally to temperature elevation and, consequently, HIFU power.

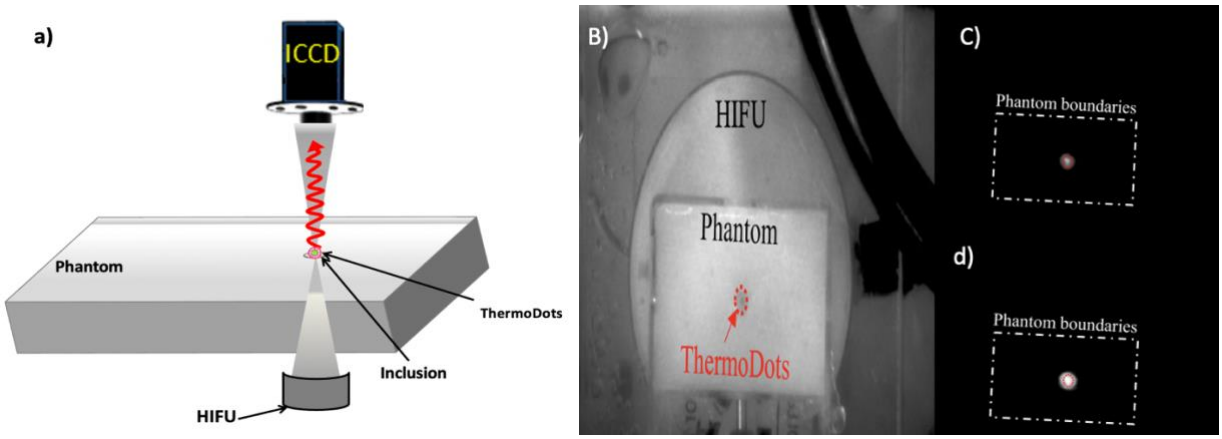

Figure 4.5: a) The 3D schematic of a phantom with respect to ICCD camera and HIFU location. b) Top view of the phantom placed on the imaging membrane. ICCD pictures captured at c) 1 ^{o}C and d) 2 ^{o}C temperature elevation.

4.2 ICCD based TM-FT data acquisition

4.2.1 Conventional FDOT data acquisition

An ultra-thin membrane that is transparent to both optical and ultrasonic radiation is used to support the object being studied. Before staring the experiment, the ICCD based TM-FT system is tested by initiating a 2-second low power HIFU pulse. This quick HIFU test is used to ensure correct placement of the phantom, analyze the change in the signal intensity to make sure there wouldn't be any agent leakage, adjust the intensity level of HIFU pulse, and lastly to confirm temperature responsiveness of ThermoDots. The graph in Figure 4.6a represents the signal change during the HIFU pulse, and images labeled by I, II and III

represents ICDD images taken while HIFU is off, during HIFU pulse, and during cooling phase, when HIFU is turned off again after the 2-second pulse.

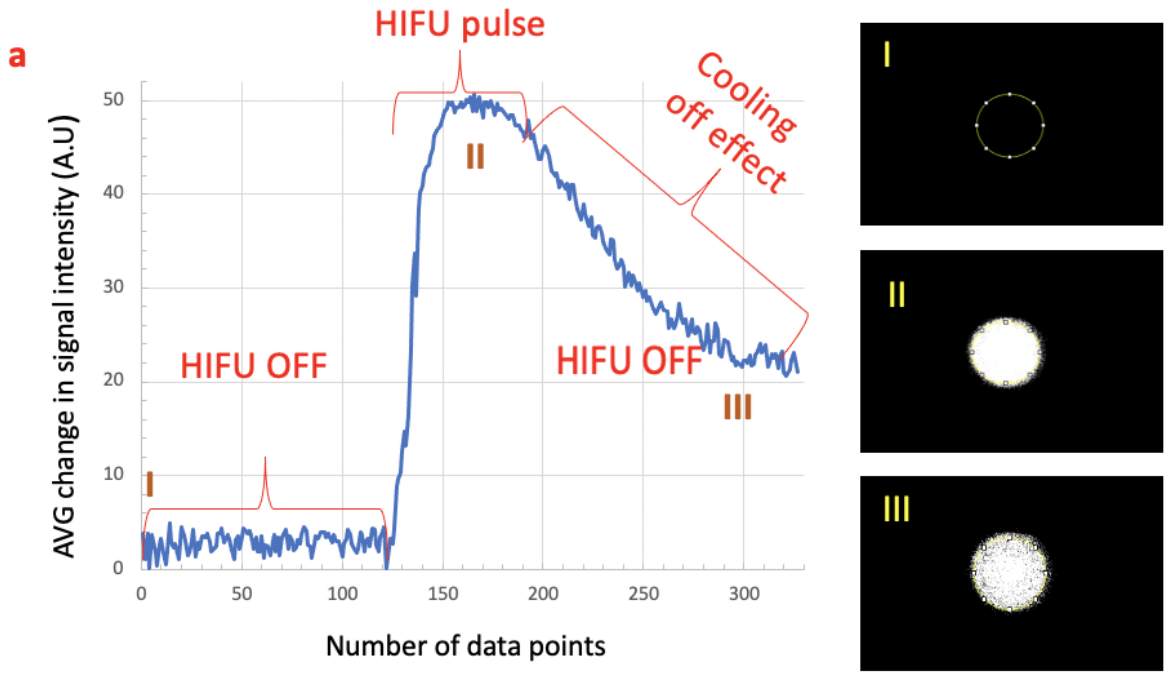

Figure 4.6: Illustration of signal change when the HIFU is off, during the HIFU pulse and the cooling phase. Corresponding ICCD images for selected time points are given at the right. Labeled by I, II, and III.

After testing the experimental set up using a translational stage, a 785 nm excitation laser beam is scanned over a 7 × 5 grid from the bottom of the membrane, while CCD images are taken from the top. The excitation light is blocked by an 830+/-10 nm bandpass filter, which allows the camera to detect only the fluorescence emission ThermoDots. This 7 x 5 grid is represented by a total of 35 images. The excitation light is turned on and a fluorescence image is recorded using a 500 ms integration time and an average of four images at each grid point (5 mm apart). For the traditional FDOT, the total imaging duration, including positioning, is close to one minute. Acquiring DOT data, which offers the optical

absorption map, is also crucial to enhancing the FDOT's accuracy. On the same grid, DOT data is progressively collected without the use of a bandpass fluorescence filter using a 785 nm and an 830 nm laser [91]. These additional DOT scans are also finished in less than a minute. The measurements are then subjected to a standard FDOT reconstruction method to determine the location of the inclusion, also called the region of interest (ROI). This provides an *a priori* mask for the TM-FT scan. The accuracy of the FDOT inverse solver is later improved by using the absorption maps that are reconstructed by the DOT inverse solver at the excitation and emission wavelengths of the ThermoDots.

4.2.2 ICCD based TM-FT scan to create functional priori

After completing FDOT data acquisition and image reconstruction, a ROI is chosen on the traditional FDOT pictures by using a threshold at full-width-half-maximum (FWHM). Afterwards, the TM-FT scan is performed using high intensity focused ultrasound. This time only the ROI region is being scanned and at each point the HIFU is being activated as well. For this purpose, a 5x5 points region is being scanned through, with the points being 0.5 mm apart from each other for a better precision, which brings the total number of the points to 25. Additionally, in this scan turning the HIFU for 2-second low power pulse from the HIFU modifies the temperature of the region by a few degrees at each point. Figure 4.7 illustrates an example of the image reconstruction process using a phantom study to reconstruct a 3-mm-diameter inclusion filled with ThermoDots. Figure 4.7a shows the cross-sectional view of the actual distribution of the ThermoDots. Figure 4.7d shows the reconstructed distribution for the same area using the traditional FDOT. As previously seen in Figure 4.7d the 3 mm inclusion cannot be recovered by the usual FDOT because of low resolution.

Therefore, once the ROI has been chosen with FDOT scan, an HIFU scan is carried out while a significantly denser grid with 0.65mm steps (i.e., half the HIFU beam size of 1.3 mm is placed on the ROI. Figure 4.7b is an illustration of the ROI chosen at FWHM features a green solid-line contour.

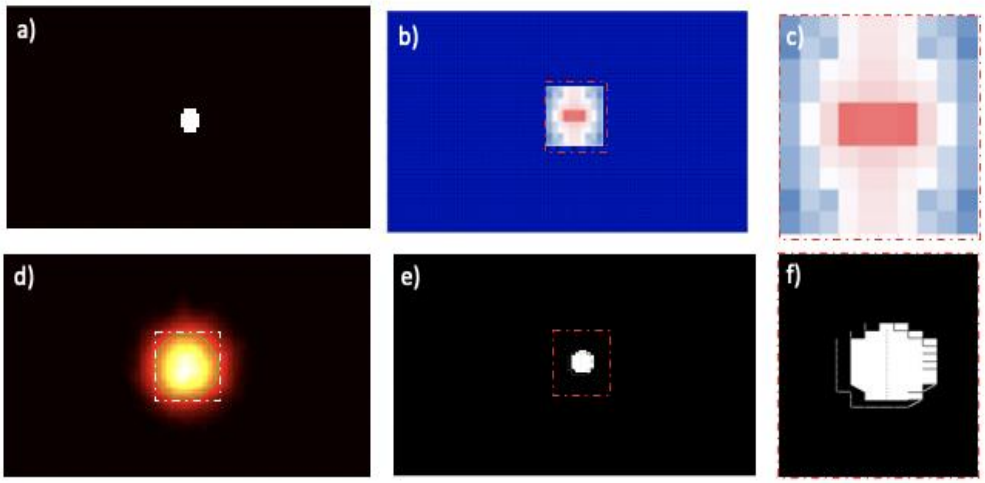

Figure 4.7: The steps of the TMFT functional a priori mask recovery is demonstrated using an example medium that has an inclusion with a 3-mm diameter and ThermoDots inside of it. a) Binary map displaying the inclusion's actual position. b) traditional FDOT, by segmenting the image at the FWHM, a ROI is defined over the FDOT image (Green solid-line contour). The FDOT segmented ROI, which is shown with the square with the white dashed line, is surrounded by a rectangle ROI. c) a fluorescence signal variation map generated by utilizing a step-and-shoot mode to scan the HIFU over the rectangle ROI. d) examining the signal variation map in more detail. e) The fluorescence variation map is segmented to create a binary map. f) A closer inspection reveals the recovered inclusion's outline.

By focusing the acoustic waves, the HIFU transducer produces a zone of high heat at its focal zone. The targeted area can be warmed up with only a small impact on the tissues around it due to this localized heating (<2 ^{o}C). Using focused ultrasound in the low power mode, TMFT produces a brief, minimal warmth. The excitation light and focused ultrasound beam are swept across this dense grid during the TMFT HIFU scanning while the fluorescence emission data is recorded with the ICCD camera, initially without and then after a brief HIFU pulse. In this case, 25 data points are used over a 5 × 5 grid, bringing the overall HIFU scan

time to under three minutes. The signal intensifies when the HIFU beam hits the ThermoDots, confirming their presence [33, 86]. A binary mask is built over this dense grid using this fluctuation in the fluorescence emission signal recorded by the ICCD, as shown in Figure 4.7e. Moreover, Figure 4.7f provides a closer look at this binary mask. In contrast to the traditional structural a priori generated from anatomic imaging modalities, this binary mask directly maps the fluorophore distribution and has a substantially greater resolution than the ROI determined by low resolution FDOT [32, 40, 86, 92-95]. When compared to FDOT alone or when paired with an anatomical imaging technique approach, TMFT can offer significantly higher quantitative accuracy and high spatial due to the use of a soft a priori approach.

4.3 Mathematical modeling and Image reconstruction algorithm used for TM-FT

Similar to conventional FDOT, coupled diffusion equations are used to predict the propagation of excitation light, its absorption by the fluorophore and conversion to emission light, and finally the propagation of the latter inside the imaged medium [23, 96-99]. Since TMFT has the advantage of using temperature-sensitive fluorophores, the right-hand side of the second equation is modified to include a thermally dependent quantum yield of fluorescence, denoted by the symbol $\eta(T)$. *As a result, the modified forward problem of TMFT enables the calculations of the density of emission photons* Φ_m^T *released by ThermoDots at temperature T [33, 86]:*

$$\begin{cases} \nabla[D_x \nabla \Phi_x(r)] - (\mu_{ax} + \mu_{af})\Phi_x(r) = -q_0(r) \\ \nabla[D_m \nabla \Phi_m^T(r)] - \mu_{am}\Phi_m^T(r) = -\Phi_x(r)\eta(T)\mu_{af} \end{cases} \quad (8)$$

The molecular extinction coefficient and fluorophore concentration are represented by the letters ε and C, respectively, and $\mu_{af} = 2.303.\varepsilon.C$ *is the fluorescence absorption coefficient. The excitation photon density is x(r).* $D = \frac{1}{3(\mu_a + \mu_s')}$ *is the formula for the diffusion coefficient, where* μ_a *and* μ_s' *are the medium's absorption and reduced scattering coefficients, respectively [33, 100]. The excitation and emission wavelengths are denoted by the subscripts x and m, respectively. The inverse problem, whose goal is to reduce the discrepancy between the fluorescence fluence recorded at the medium's surface and the one calculated by answering Eq. 8, is solved to reconstruct the TMFT images.*

$$\Omega(\mu_{af}) = \sum_{i=1}^{N_s} \sum_{j=1}^{N_d} \left(\Im_{ij}^T - F_{ij}^T(\mu_{af})\right)^2 \quad (9)$$

Where $F_{ij}^T(\mu_{af})$ *is the set of simulated emission light fluence, which is determined by resolving the forward problem posed by Eq. 8.* $\Im_{ij}^T$ is the set of emission light fluence recorded at temperature T. The total number of sources and detectors is denoted by the letters N_s and N_d, respectively. Furthermore, Levenberg-Marquardt approach is used to minimize the cost function in Eq. 9 while iteratively updating the vector of unknowns μ_{af} [67, 96, 98, 101-103]:

$$X_{n+1} = X_n + (J^T J + \lambda I)^{-1} J^T (\Im - F) \quad (10)$$

where J is the Jacobian matrix and X stands for the unknown vector of μ_{af}. The Jacobian matrix is J. However, the final reconstructed μ_{af} map is not quantitatively precise and is not able to retrieve the fluorescence targets with fine spatial resolution. A penalty matrix

defining the binary mask retrieved by the HIFU scan is built to include the TMFT soft a priori information [96]. The following steps can be used to obtain the penalty matrix L:

$$L_{ij} = \begin{cases} 0 & \text{i and j not in the same region} \\ -\frac{1}{N_r} & \text{i and j in the same region} \\ 1 & i = j \end{cases} \quad (11)$$

The number of nodes in each area r is denoted by the symbol N_r. Then, using the a priori knowledge that directs and constrains the conversion of the image reconstruction method, the penalty matrix, *L,* is added into the FDOT inverse problem and solved a second time. Once more, the Levenberg-Marquardt approach is used to update the unknown μ_{af} while the inverse issue is iteratively solved:

$$X_{n+1} = X_n + (J^T J + \lambda L^T L)^{-1} J^T (\Im - F) \quad (12)$$

The fluorescence images' quality is much enhanced by solving the inverse problem as stated by Eq.12, which enables the achievement of much higher quantitative precision.

4.4 ICCD based TMFT experimental results

We examine the capability of our ICCD-based TMFT system to precisely retrieve the size, shape, position, and concentration of inclusions inserted inside tissue-like agarose phantoms and filled with ThermoDots. As illustrated before in Figure 4.5a a rectangular 50 x 30 x 17 mm^3 agarose gel phantom is used. The agarose gel is treated with intralipid (0.5%) and India ink to set the phantoms' absorption and decreased scattering coefficients at 0.01 mm^{-1} and 0.8 mm^{-1}, respectively [91, 104]. The bottom center of the phantoms is designated as the origin of the spatial coordinates. A 3-mm-diamter and 10-mm-high cylindrical glass tube is

first inserted at the center of the first phantom along the z-axis i to produce a zone with ThermoDots accumulating within the phantoms. The top edge of the tube is 4 mm below the phantom's upper surface.

The real values are compared with the fluorescence absorption maps recovered with traditional FDOT and TMFT that are directly related to the ThermoDots distribution. A series of DOT data is first collected without any filters in front of the camera lens to retrieve the phantom's absorption and reduced scattering coefficients [49]. The DOT data is only collected at the excitation wavelength, 785 nm, because the absorption and scattering coefficients of the phantom at the excitation and emission wavelengths are roughly equal (~1% difference). Moreover, the optical properties of the background is set to μ_a=0.011 mm^{-1} and μ_s'= 0.81 mm^{-1}. Following the acquisition of traditional FDOT measurements, the recovered optical properties using DOT are utilized in the conventional FDOT reconstruction procedure, as optical functional *a priori* knowledge. After that, the HIFU is scanned to provide a binary mask with high spatial resolution characterizing the position and the shape of the implanted tube. Finally, using Eq. 11 and the TMFT reconstruction process, the resultant binary map is implemented as a soft a priori to determine the concentration of the ThermoDots.

Figure 4.8 displays the outcomes produced by the initial phantom with the single 3-mm-diameter inclusion. Figures 4.8b and 4.8c respectively illustrate the reconstructed fluorescence absorption maps of the ThermoDots (μ_{af}) using conventional FDOT and TMFT. The inclusion is successfully localized by FDOT; however, a sizable bright glob surrounds it. As a result, the fluorescence absorption is significantly underrepresented at 0.053±0.030

mm^{-1}, with an inaccuracy of 80%. This is mostly because the recovered fluorescence is assigned to a region that is bigger than the actual volume of a cylindrical 3-mm-diameter tube. Using various regularization parameters and initial fluorophore values, each image reconstruction is repeated five times to determine the standard deviation.

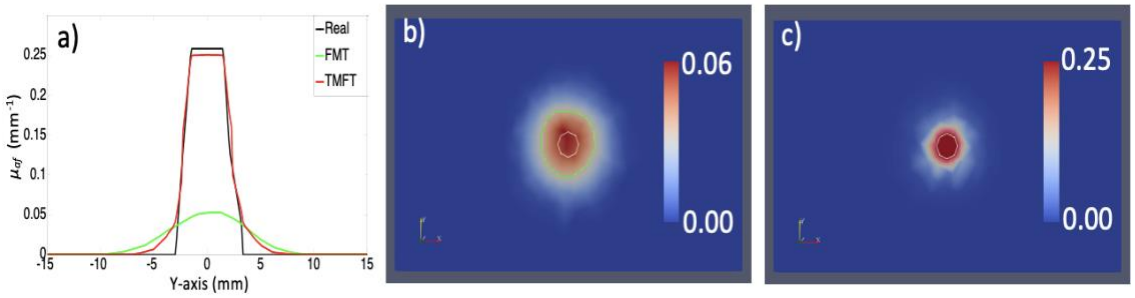

Figure 4.8: a) Shows the profiles of the fluorescence absorption along the Y-axis: Real (black), recovered using conventional FDOT (green), and TMFT (red). Cross-section of the fluorescence absorption reconstructed using b) conventional FDOT, and c) TMFT, at z=0 mm.

In contrast, the inclusion is precisely localized before any reconstruction is done by the TMFT HIFU-derived binary mask. This binary mask is utilized as soft *a priori* to solve the FDOT inverse problem to recover the concentration of ThermoDots inside the tube [33, 67, 95, 105]. In comparison to conventional FDOT, the resulting TMFT fluorescence absorption map shows improved spatial-resolution and quantitative accuracy, Figure 4.8c. The actual fluorescent inclusion's size, shape, and location are all accurately recovered by TMFT, and the fluorescence absorption is recovered with excellent accuracy at 0.255 mm^{-1}, which translates to an inaccuracy of less than 2%. Since TMFT uses focused ultrasound waves instead of optical waves, it is not restricted by the same scattering and absorption issues as optical waves. As a result, TMFT is superior in recovering the proper size, shape, and location of the ThermoDots, as seen in Figure 4.8c. Moreover, contrary to conventional FDOT, the

actual borders of the tube containing Thermodots serve as the primary confinement for the TMFT fluorescence distribution. As shown in Figure 4.8a, profiles are run along the Y-axis to better observe how the reconstructed FDOT pictures are improved by the TMFT. Traditional FDOT significantly underestimated the tube's diameter and retrieved a sizable blob with an average diameter of 7.4 mm. On the other hand, TMFT almost accurately determined the tube's diameter, with a 0.5 mm error. These studies validated the ICCD-based TM-FT prototype and confirmed that the TM-FT data acquisition and image reconstruction processes are optimized.

CHAPTER 5: Conclusion and Future Work

FDOT is distinguished from other optical molecular imaging techniques by its great sensitivity, low cost, safety, and reliability. As a result, it has emerged as the primary optical molecular imaging technique for preclinical research. Even though 2D planar fluorescence imaging is used in most investigations, more accurate animal models including orthotopic and transgenic models demand 3D tomographic imaging. The FDOT's resolution, however, is what prevents its widespread usage. Utilizing temperature-sensitive contrast agents and HIFU's highly localized heating capacity is an innovative method of enhancing the FDOT resolution. However, for efficient integration in a preclinical research setting, the dedicated apparatus should be a practical and high throughput one.

Unfortunately, our earlier fiber based TMFT system required submerging the animal in optical matching fluids. With the current design using an ICCD camera, this issue is resolved by placing the object under study on an ultrasound- and light-transparent membrane. With phantoms that mimicked animal tissue, the ICCD-based system was validated in this thesis. Like the fiber-based technology, the CCD-based TM-FT system is superior to conventional FDOT. High spatial resolution of the TMFT resulted in a significant improvement in quantitative accuracy.

The next step would be testing the ICCD based system *in vivo* using Thermodots . However, the responsive range of Themodots made using F-127 Pluronic powder is 17-23°C and this range is not suitable for animal studies. In vivo studies usually are performed on mice since their body temperature is around 30-32 °C under anesthesia. This issue can be

solved relatively easily since a range of Pluronic types with various thermal properties, in vivo characteristics, and biological interactions with cells and cell membranes can be produced by adjusting the lengths of the polymer blocks [81].

5.1 Future work

Phantom studies have been completed using rectangular phantoms. To recover the irregular boundary of small animals, the next step will be integrating a structured light illumination. This scheme will allow ICCD to delineate the irregular boundary of the small animal, which will be used for the image reconstruction purpose. With this upgrade, ICCD-based TMFT will be ready for *in vivo* preclinical research. Meanwhile, The ThremoDots should also be modified also optimized to work around 30-32^{o}C.

Since ICG and some polymers, the two main ingredients used to synthesize ThermoDots, are FDA-approved, TMFT has a great potential for clinical translation as well. Furthermore, TMFT is an excellent option for deep tissue optical clinical imaging due to the quick synthesis of specific molecular probes for human imaging, such prostate cancer imaging.

Furthermore, as the one of the main components of the TM-FT, HIFU is a new and promising minimally invasive therapeutic option in clinical arena. HIFU uses mechanically moving single-focus ultrasonic transducers to cause thermal damage and coagulative necrosis in the target tissue[70]. Because of its minimally invasive nature, single-session treatment, minimal anesthetic, and perceived short recovery period and quick return to daily activity, this approach is quickly gaining clinical recognition among urologists and patients

[106]. Long-term evidence of disease control is limited, and the potential therapeutic efficacy and progression-free survival benefit of HIFU have yet to be adequately studied. The fundamental advantage of HIFU over other minimally invasive treatments for localized prostate cancer is that it is noninvasive and requires no percutaneous needle insertion[106]. MRI and ultrasound are currently the only imaging modalities for HIFU treatment that are clinically available [107]. For real-time treatment monitoring, MRI provides high resolution imaging, making it suitable for directing and monitoring HIFU ablation [106, 107].

Utilizing prostate specific membrane antigen (PSMA) targeting ThermoDots, TM-FT can replace the MRI to guide HIFU therapy in the future. It is very promising that in the future, ThermoDots will be targeted to enable tumor-specific imaging and hence guide other therapeutic interventions beside the HIFU-based ones. However the HIFU based therapies will be the first target of the future TM-FT applications [106].

References

1. *"Optical Tomography - an overview | ScienceDirect Topics,"*

2. Ntziachristos, V., et al., *Looking and listening to light: the evolution of whole-body photonic imaging.* Nature biotechnology, 2005. **23**(3): p. 313-320.

3. Hoshi, Y. and Y. Yamada, *Overview of diffuse optical tomography and its clinical applications.* Journal of biomedical optics, 2016. **21**(9): p. 091312.

4. Durduran, T., et al., *Diffuse optics for tissue monitoring and tomography.* Reports on progress in physics, 2010. **73**(7): p. 076701.

5. Lin, Y., et al., *Quantitative fluorescence tomography using a trimodality system: in vivo validation.* J Biomed Opt, 2010. **15**(4): p. 040503.

6. Gulsen, G., et al., *Design and implementation of a multifrequency near-infrared diffuse optical tomography system.* J Biomed Opt, 2006. **11**(1): p. 14020.

7. Lin, Y., et al., *In vivo validation of quantitative frequency domain fluorescence tomography.* J Biomed Opt, 2012. **17**(12): p. 126021.

8. Unlu, M.B., Y. Lin, and G. Gulsen, *Dynamic contrast-enhanced diffuse optical tomography (DCE-DOT): experimental validation with a dynamic phantom.* Phys Med Biol, 2009. **54**(21): p. 6739-55.

9. al, P.K.Y.e., *"Structural information within regularization matrices improves near infrared diffuse optical tomography".* 2007, *Optics Express*. p. pp.8043-8058.

10. Barber, W.C., et al., *Combined fluorescence and X-Ray tomography for quantitative in vivo detection of fluorophore.* Technol Cancer Res Treat, 2010. **9**(1): p. 45-52.

11. David Thayer, M.B.U., Yuting Lin, Kevin Yan, Orhan Nalcioglu, Gultekin Gulsen, *Dual-Contrast Dynamic MRI-DOT for Small Animal Imaging.* Technology in cancer research and treatment, 2010. **9**(1): p. 10.

12. Gao, H., et al., *Fully linear reconstruction method for fluorescence yield and lifetime through inverse complex-source formulation: simulation studies.* Opt Lett, 2010. **35**(11): p. 1899-901.

13. H. Yan, Y.L., W. Barber, B. Unlu, and G. Gulsen, *A Gantry-based Tri-Modality system for Bioluminescence Tomography.* Review of Scientific Instruments, 2012. **in press**.

14. Lin, Y., et al., *Fluorescence diffuse optical tomography with functional and anatomical a priori information: feasibility study.* Phys Med Biol, 2007. **52**(18): p. 5569-85.

15. Lin, Y., et al., *Quantitative fluorescence tomography using a combined tri-modality FT/DOT/XCT system.* Optics Express, 2009. **under review**.

16. Lin, Y., et al., *Tumor characterization in small animals using magnetic resonance-guided dynamic contrast enhanced diffuse optical tomography.* J Biomed Opt, 2011. **16**(10): p. 106015.

17. Thayer, D., et al., *Dual-contrast dynamic MRI-DOT for small animal imaging.* Technol Cancer Res Treat, 2010. **9**(1): p. 61-70.

18. Unlu, M.B., et al., *Simultaneous in vivo dynamic magnetic resonance-diffuse optical tomography for small animal imaging.* J Biomed Opt, 2008. **13**(6): p. 060501.

19. Y Lin, D.T., O Nalcioglu and G Gulsen,, *Tumor Characterization in Small Animals Using MR-guided Dynamic Contrast Enhanced Diffuse Optical Tomography (DCE-DOT).* Journal of Biomedical Optics, 2011. **In press**.

20. Lin, Y., et al., *A photo-multiplier tube-based hybrid MRI and frequency domain fluorescence tomography system for small animal imaging.* Phys Med Biol, 2011. **56**(15): p. 4731-47.

21. Lin, Y., et al., *Temperature-modulated fluorescence tomography based on both concentration and lifetime contrast.* J Biomed Opt, 2012. **17**(5): p. 056007.

22. Keren, S., et al., *A comparison between a time domain and continuous wave small animal optical imaging system.* IEEE transactions on medical imaging, 2007. **27**(1): p. 58-63.

23. Erkol, H., et al., *An extended analytical approach for diffuse optical imaging.* Physics in Medicine & Biology, 2015. **60**(13): p. 5103.

24. Erkol, H., et al., *Comprehensive analytical model for CW laser induced heat in turbid media.* Opt Express, 2015. **23**(24): p. 31069-84.

25. Gurfinkel, M., et al., *Near-infrared fluorescence optical imaging and tomography.* Disease Markers, 2004. **19**(2-3): p. 107-121.

26. Kumar, A.T., et al., *Comparison of frequency-domain and time-domain fluorescence lifetime tomography.* Optics letters, 2008. **33**(5): p. 470-472.

27. Nissilä, I.T., et al., *Comparison between a time-domain and a frequency-domain system for optical tomography.* Journal of biomedical optics, 2006. **11**(6): p. 064015.

28. Lee, J. and E.M. Sevick-Muraca, *Three-dimensional fluorescence enhanced optical tomography using referenced frequency-domain photon migration measurements at emission and excitation wavelengths.* JOSA A, 2002. **19**(4): p. 759-771.

29. Suhling, K., et al., *Imaging the environment of green fluorescent protein.* Biophysical journal, 2002. **83**(6): p. 3589-3595.

30. Kuwana, E. and E.M. Sevick-Muraca, *Fluorescence lifetime spectroscopy for pH sensing in scattering media.* Analytical chemistry, 2003. **75**(16): p. 4325-4329.

31. Kwong, T.C., et al., *Experimental evaluation of the resolution and quantitative accuracy of temperature-modulated fluorescence tomography.* Appl Opt, 2017. **56**(3): p. 521-529.

32. Nouizi, F., et al. *A combined HIFU-Fluorescence Tomography high-resolution imaging technique using temperature-modulated thermodots*. in *Novel Techniques in Microscopy*. 2013. Optica Publishing Group.

33. Nouizi, F., et al., *Implementation of a new scanning method for high-resolution fluorescence tomography using thermo-sensitive fluorescent agents.* Optics letters, 2015. **40**(21): p. 4991-4994.

34. Y. An, K.W., and J. Tian, *"Recent methodology advances in fluorescence molecular tomography,"* Sep. 2018, *Visual Computing for Industry, Biomedicine, and Art* , .

35. Faulkner, D., et al., *Diffuse Fluorescence Tomography.* 2021.

36. Leblond, F., et al., *Pre-clinical whole-body fluorescence imaging: Review of instruments, methods and applications.* Journal of photochemistry and photobiology B: Biology, 2010. **98**(1): p. 77-94.

37. Stuker, F., J. Ripoll, and M. Rudin, *Fluorescence molecular tomography: principles and potential for pharmaceutical research.* Pharmaceutics, 2011. **3**(2): p. 229-274.

38. Lin, Y.T., et al., *A Hybrid Fluorescence Tomography and X-ray CT System for Quantitative Molecular Imaging.* Multimodal Biomedical Imaging V, 2010. **7557**.

39. Lin, Y., et al., *Quantitative fluorescence tomography using a combined tri-modality FT/DOT/XCT system.* Opt Express, 2010. **18**(8): p. 7835-50.

40. Lin, Y., et al., *Temperature-modulated fluorescence tomography based on both concentration and lifetime contrast.* Journal of biomedical optics, 2012. **17**(5): p. 056007.

41. Lin, Y., et al., *Temperature-modulated fluorescence tomography in a turbid media.* Appl Phys Lett, 2012. **100**(7): p. 73702-737024.

42. Lin, Y., et al., *Photo-magnetic imaging: resolving optical contrast at MRI resolution.* Phys Med Biol, 2013. **58**(11): p. 3551-62.

43. Thayer, D.A., et al., *Laser-induced photo-thermal magnetic imaging.* Appl Phys Lett, 2012. **101**(8): p. 83703.

44. Giepmans, B.N.G., *"The Fluorescent Toolbox for Assessing Protein Location and Function",*. Apr. 2006, *Science* ,. p. pp. 217–224.

45. Polom, W., et al., *Multispectral Imaging Using Fluorescent Properties of Indocyanine Green and Methylene Blue in Colorectal Surgery—Initial Experience.* Journal of Clinical Medicine, 2022. **11**(2): p. 368.

46. Kwong, T.C., et al. *Activatable thermo-sensitive ICG encapsulated Pluronic nanocapsules for temperature sensitive fluorescence tomography*. in *Reporters, Markers, Dyes, Nanoparticles, and Molecular Probes for Biomedical Applications VII*. 2015. SPIE.

47. Kunjachan, S., et al., *Passive versus active tumor targeting using RGD-and NGR-modified polymeric nanomedicines.* Nano letters, 2014. **14**(2): p. 972-981.

48. Hellebust, A. and R. Richards-Kortum, *Advances in molecular imaging: targeted optical contrast agents for cancer diagnostics.* Nanomedicine, 2012. **7**(3): p. 429-445.

49. Quek, C.-H. and K.W. Leong, *Near-infrared fluorescent nanoprobes for in vivo optical imaging.* Nanomaterials, 2012. **2**(2): p. 92-112.

50. Kobayashi, H. and P.L. Choyke, *Target-cancer-cell-specific activatable fluorescence imaging probes: rational design and in vivo applications.* Accounts of chemical research, 2011. **44**(2): p. 83-90.

51. Chen, X., *Molecular imaging probes for cancer research*. 2012: World Scientific.

52. D Nolting, D., J. C Gore, and W. Pham, *Near-infrared dyes: probe development and applications in optical mole-cular imaging.* Current organic synthesis, 2011. **8**(4): p. 521-534.

53. Kim, T.H., et al., *Evaluation of temperature-sensitive, indocyanine green-encapsulating micelles for noninvasive near-infrared tumor imaging.* Pharmaceutical research, 2010. **27**(9): p. 1900-1913.

54. Urano, Y., et al., *Selective molecular imaging of viable cancer cells with pH-activatable fluorescence probes.* Nature medicine, 2009. **15**(1): p. 104-109.

55. Lee, H., et al., *Near-infrared pH-activatable fluorescent probes for imaging primary and metastatic breast tumors.* Bioconjugate chemistry, 2011. **22**(4): p. 777-784.

56. Chen, Y. and X. Li, *Near-infrared fluorescent nanocapsules with reversible response to thermal/pH modulation for optical imaging.* Biomacromolecules, 2011. **12**(12): p. 4367-4372.

57. Kiyose, K., et al., *Hypoxia-sensitive fluorescent probes for in vivo real-time fluorescence imaging of acute ischemia.* Journal of the American Chemical Society, 2010. **132**(45): p. 15846-15848.

58. Lee, S., et al., *Activatable imaging probes with amplified fluorescent signals.* Chemical communications, 2008(36): p. 4250-4260.

59. J. McEwen, *"Jablonksi Diagram",* . 2016, Chemistry LibreTexts.

60. Lichtman, J.W. and J.-A. Conchello, *Fluorescence microscopy.* Nature methods, 2005. **2**(12): p. 910-919.

61. Valeur, B. and M.N. Berberan-Santos, *Molecular fluorescence: principles and applications*. 2012: John Wiley & Sons.

62. Maarek, J.-M.I. and D.P. Holschneider, *Estimation of indocyanine green concentration in blood from fluorescence emission: application to hemodynamic assessment during hemodialysis.* Journal of biomedical optics, 2009. **14**(5): p. 054006.

63. Hollins, B., B. Noe, and J. Henderson, *Fluorometric determination of indocyanine green in plasma.* Clinical chemistry, 1987. **33**(6): p. 765-768.

64. Godavarty, A., E.M. Sevick-Muraca, and M.J. Eppstein, *Three-dimensional fluorescence lifetime tomography.* Medical physics, 2005. **32**(4): p. 992-1000.

65. Meyvis, T.K., et al., *Fluorescence recovery after photobleaching: a versatile tool for mobility and interaction measurements in pharmaceutical research.* Pharmaceutical research, 1999. **16**(8): p. 1153-1162.

66. Landragin-Frassati, A., et al., *Application of a wavelet-Galerkin method to the forward problem resolution in fluorescence diffuse optical tomography.* Opt Express, 2009. **17**(21): p. 18433-48.

67. Kwong, T.C., et al., *Feasibility study of high spatial resolution multimodality fluorescence tomography in ex vivo biological tissue.* Applied optics, 2017. **56**(28): p. 7886-7891.

68. Xu, C.T., et al., *High-resolution fluorescence diffuse optical tomography developed with nonlinear upconverting nanoparticles.* ACS nano, 2012. **6**(6): p. 4788-4795.

69. Cochran, J.M., et al., *Hybrid time-domain and continuous-wave diffuse optical tomography instrument with concurrent, clinical magnetic resonance imaging for breast cancer imaging.* Journal of biomedical optics, 2019. **24**(5): p. 051409.

70. *"Emerging Role of HIFU as a Noninvasive Ablative - ProQuest,"*. www.proquest.com . .

71. Mehrabi, M., et al. *CCD-based temperature modulated fluorescence tomography*. in *Optical Tomography and Spectroscopy of Tissue XIII*. 2019. SPIE.

72. Tsenova, V. and E.V. Stoykova. *Refractive index measurement in human tissue samples*. in *12th International School on Quantum Electronics: Laser Physics and Applications*. 2003. SPIE.

73. Gulsen, G., et al., *Modulating tissue temperature for high-resolution, in vivo fluorescence tomography.*

74. Escobar-Chávez, J., et al., *Applications of thermo-reversible pluronic F-127 gels in pharmaceutical formulations.* Journal of Pharmacy & Pharmaceutical Sciences, 2006. **9**(3): p. 339-58.

75. Bremer, C., V. Ntziachristos, and R. Weissleder, *Optical-based molecular imaging: contrast agents and potential medical applications.* European radiology, 2003. **13**(2): p. 231-243.

76. Desmettre, T., J. Devoisselle, and S. Mordon, *Fluorescence properties and metabolic features of indocyanine green (ICG) as related to angiography.* Survey of ophthalmology, 2000. **45**(1): p. 15-27.

77. al., M.O.e., *"In vivo molecular imaging of cancer with a quenching near-infrared fluorescent probe using conjugates of monoclonal antibodies and indocyanine green,"*. 2009, *Cancer research* **69**. p. pp. 1268-1272.

78. Licha, K., et al., *Hydrophilic Cyanine Dyes as Contrast Agents for Near-infrared Tumor Imaging: Synthesis, Photophysical Properties and Spectroscopic In vivo Characterization¶.* Photochemistry and photobiology, 2000. **72**(3): p. 392-398.

79. Saxena, V., M. Sadoqi, and J. Shao, *Enhanced photo-stability, thermal-stability and aqueous-stability of indocyanine green in polymeric nanoparticulate systems.* Journal of Photochemistry and Photobiology B: Biology, 2004. **74**(1): p. 29-38.

80. Hammouda, B. and D.L. Ho, *Insight into chain dimensions in PEO/water solutions.* Journal of Polymer Science Part B: Polymer Physics, 2007. **45**(16): p. 2196-2200.

81. Chandaroy, P., et al., *Utilizing temperature-sensitive association of Pluronic F-127 with lipid bilayers to control liposome–cell adhesion.* Biochimica et Biophysica Acta (BBA)-Biomembranes, 2002. **1559**(1): p. 32-42.

82. Batrakova, E.V. and A.V. Kabanov, *Pluronic block copolymers: evolution of drug delivery concept from inert nanocarriers to biological response modifiers.* Journal of controlled release, 2008. **130**(2): p. 98-106.

83. al., V.B.R.e., *"Encapsulation and stabilization of indocyanine green within poly(styrene-alt-maleic anhydride) block-poly(styrene) micelles for near-infrared imaging,"*. 2008, *Journal of Biomedical Optics* **13** (1). p. 014025-014010.

84. Foundation, F.U., *"Mechanisms of Action"*. 2015, Focused Ultrasound Foundation

85. al., Y.-s.K.e., *"High-intensity focused ultrasound therapy: an overview for radiologists."*. 2008, *Korean journal of radiology 9*. p. 291-302.

86. Lin, Y., et al., *Temperature-modulated fluorescence tomography in a turbid media.* Applied physics letters, 2012. **100**(7): p. 073702.

87. *"ICCD System Overview" stanfordcomputeroptics.com* .

88. I. D. Johnson, a.M.W.D., *"Jablonski Energy Diagram, in Optical Microscopy Primer Specialized Techniques M. W. Davidson, Ed., Molecular Expressions*. 2003.

89. Lakowicz, J.R., *Principles of Fluorescence Spectroscopy , Third Ed ed*. 2006: Springer US, Boston, MA .

90. Jaszczak, M., *"What is a phantom? How does it work? | Data Spectrum,"* Apr. 28, 2020: *www.spect.com*.

91. Lin, Y., et al., *Fluorescence diffuse optical tomography with functional and anatomical a priori information: feasibility study.* Physics in Medicine & Biology, 2007. **52**(18): p. 5569.

92. Kwong, T.C., et al. *Temperature-modulated fluorescence tomography: modulating tissue temperature using HIFU for high-resolution in vivo fluorescence tomography*. in *Multimodal Biomedical Imaging VIII*. 2013. SPIE.

93. Kwong, T.C., et al. *Validation of temperature-modulated fluorescence tomography in vivo*. in *Multimodal Biomedical Imaging IX*. 2014. SPIE.

94. Kwong, T.C., et al. *Thermal Outlining using Focused Ultrasound (TOFU) with reversible temperature sensitive fluorescent probes*. in *Multimodal Biomedical Imaging XI*. 2016. SPIE.

95. Kwong, T.C., et al., *Experimental evaluation of the resolution and quantitative accuracy of temperature-modulated fluorescence tomography.* Applied optics, 2017. **56**(3): p. 521-529.

96. Arridge, S.R., *Optical tomography in medical imaging.* Inverse problems, 1999. **15**(2): p. R41.

97. Nouizi, F., et al., *An accelerated photo-magnetic imaging reconstruction algorithm based on an analytical forward solution and a fast Jacobian assembly method.* Physics in Medicine & Biology, 2016. **61**(20): p. 7448.

98. Nouizi, F., et al., *Experimental validation of a high-resolution diffuse optical imaging modality: photomagnetic imaging.* Journal of Biomedical Optics, 2016. **21**(1): p. 016009.

99. Nouizi, F., et al., *Real-time photo-magnetic imaging.* Biomedical optics express, 2016. **7**(10): p. 3899-3904.

100. Nouizi, F., et al. *3D modeling for solving forward model of no-contact Fluorescence Diffuse Optical Tomography method*. in *European Conference on Biomedical Optics*. 2009. Optica Publishing Group.

101. Nouizi, F., et al., *Improvement of absorption and scattering discrimination by selection of sensitive points on temporal profile in diffuse optical tomography.* Optics express, 2011. **19**(13): p. 12843-12854.

102. Levenberg, K., *A method for the solution of certain non-linear problems in least squares.* Quarterly of applied mathematics, 1944. **2**(2): p. 164-168.

103. Nouizi, F., et al., *Analytical Photo Magnetic Imaging, Optical Tomography and Spectroscopy, Optical Society of America, 2016, p*. OW4D.

104. Wan, W., et al., *Region-based diffuse optical tomography with registered atlas: in vivo acquisition of mouse optical properties.* Biomedical Optics Express, 2016. **7**(12): p. 5066-5080.

105. Lin, Y., et al., *Simulation-based evaluation of the resolution and quantitative accuracy of temperature-modulated fluorescence tomography.* Applied optics, 2015. **54**(25): p. 7612-7621.

106. Barqawi, A.B. and E.D. Crawford, *Emerging role of HIFU as a noninvasive ablative method to treat localized prostate cancer.* Oncology, 2008. **22**(2): p. 123.

107. Orsi, F., et al., *High intensity focused ultrasound ablation: a new therapeutic option for solid tumors.* Journal of cancer research and therapeutics, 2010. **6**(4): p. 414.